iScience

CellPress
OPEN ACCESS

Article

Membrane Estrogen Receptor (GPER) and Follicle-Stimulating Hormone Receptor (FSHR) Heteromeric Complexes Promote Human Ovarian Follicle Survival

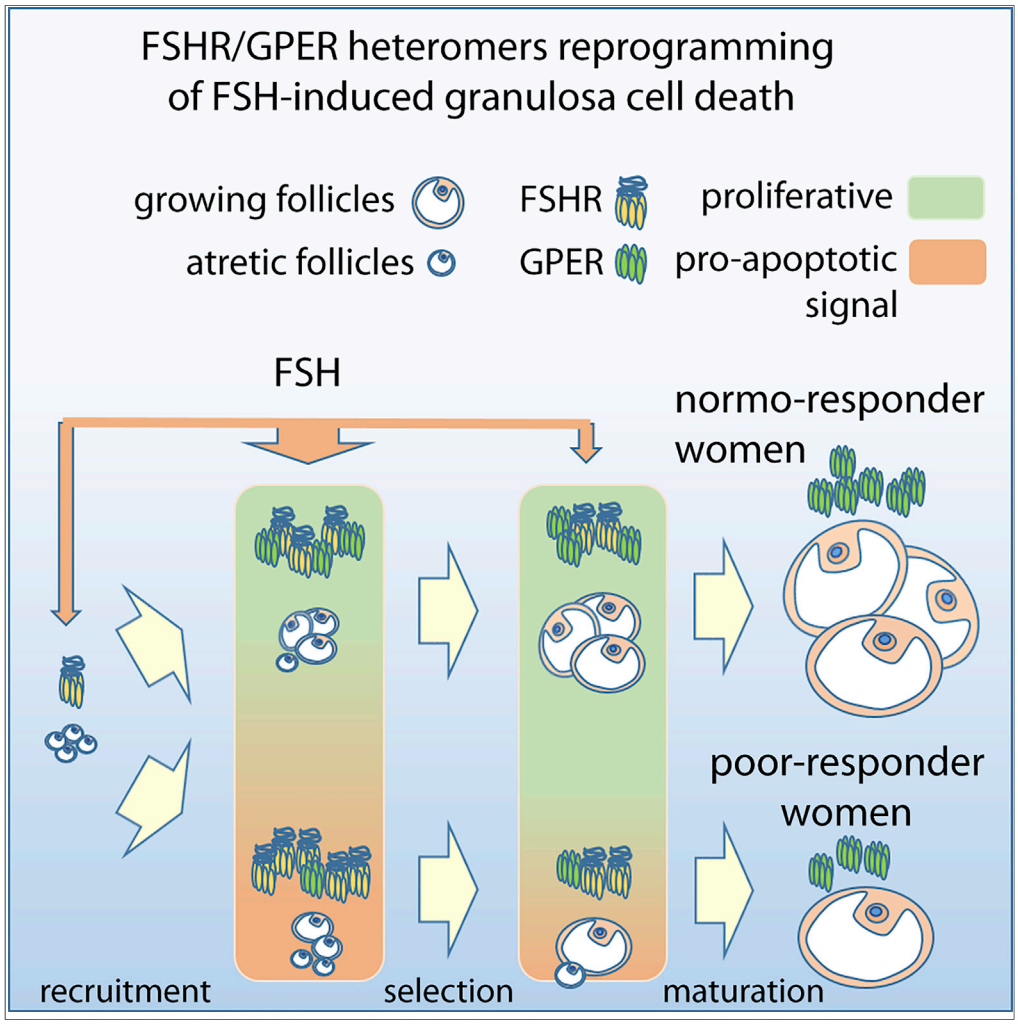

Livio Casarini, Clara Lazzaretti, Elia Paradiso, ..., Adolfo Rivero-Müller, Aylin C. Hanyaloglu, Manuela Simoni

livio.casarini@unimore.it

HIGHLIGHTS

G-protein-coupled estrogen receptor (GPER) interacts with FSH receptor (FSHR)

FSHR/GPER heteromers reprogram FSH-induced death signals to proliferative stimuli

Anti-apoptotic signaling of heteromers is via a GPER-Gαs inhibitory complex and Gβγ

Heteromer formation impacts follicle maturation and FSH responses of IVF patients

Casarini et al., iScience *23*, 101812
December 18, 2020
https://doi.org/10.1016/j.isci.2020.101812

iScience

CellPress
OPEN ACCESS

Article

Membrane Estrogen Receptor (GPER) and Follicle-Stimulating Hormone Receptor (FSHR) Heteromeric Complexes Promote Human Ovarian Follicle Survival

Livio Casarini,[1,2,18,*] Clara Lazzaretti,[1,3] Elia Paradiso,[1,3] Silvia Limoncella,[1] Laura Riccetti,[1] Samantha Sperduti,[1,2] Beatrice Melli,[1] Serena Marcozzi,[4] Claudia Anzivino,[1] Niamh S. Sayers,[5] Jakub Czapinski,[6,7] Giulia Brigante,[1,8] Francesco Potì,[9] Antonio La Marca,[10,11] Francesco De Pascali,[12] Eric Reiter,[12] Angela Falbo,[13] Jessica Daolio,[13] Maria Teresa Villani,[13] Monica Lispi,[3,14] Giovanna Orlando,[15] Francesca G. Klinger,[4] Francesca Fanelli,[16,17] Adolfo Rivero-Müller,[6] Aylin C. Hanyaloglu,[5] and Manuela Simoni[1,2,8,12]

SUMMARY

Classically, follicle-stimulating hormone receptor (FSHR)-driven cAMP-mediated signaling boosts human ovarian follicle growth and oocyte maturation. However, contradicting *in vitro* data suggest a different view on physiological significance of FSHR-mediated cAMP signaling. We found that the G-protein-coupled estrogen receptor (GPER) heteromerizes with FSHR, reprogramming cAMP/death signals into proliferative stimuli fundamental for sustaining oocyte survival. In human granulosa cells, survival signals are missing at high FSHR:GPER ratio, which negatively impacts follicle maturation and strongly correlates with preferential Gαs protein/cAMP-pathway coupling and FSH responsiveness of patients undergoing controlled ovarian stimulation. In contrast, FSHR/GPER heteromers triggered anti-apoptotic/proliferative FSH signaling delivered via the Gβγ dimer, whereas impairment of heteromer formation or GPER knockdown enhanced the FSH-dependent cell death and steroidogenesis. Therefore, our findings indicate how oocyte maturation depends on the capability of GPER to shape FSHR selective signals, indicating hormone receptor heteromers may be a marker of cell proliferation.

INTRODUCTION

Ovarian follicular growth and dominance in women of reproductive age is a physiological example of how a tightly regulated equilibrium between active cell proliferation and apoptosis results in the selection of a single dominant follicle at the expense of all others. Key players of this game are sex hormones, follitropin (FSH) and 17β-estradiol (E_2), which stimulate cell viability and proliferative signals in the gonads and certain tumor cells (Correia et al., 2015; Lizneva et al., 2019). Sex-hormone receptors are druggable targets in fertility and cancer treatment to control cell death and survival.

The FSH-receptor (FSHR) stimulates Gαs protein-dependent cAMP/PKA activation, resulting in cAMP-response element binding protein (CREB) phosphorylation and steroidogenic activity, necessary to produce estrogens that, in turn, are well-known stimulators of growth (Casarini and Crépieux, 2019). However, a pro-apoptotic role of FSH has also been proposed (Amsterdam et al., 1998, 2003), and, intriguingly, prolonged FSHR overexpression (Casarini et al., 2016) or accumulation of high intracellular cAMP levels (Aharoni et al., 1995; Yoshida et al., 2000) are a prerequisite for both steroid synthesis and cell death (Breckwoldt et al., 1996). The FSH-related pro-apoptotic activity occurs when high FSHR expression is induced (Casarini et al., 2016), providing a plausible reason why no consistent steroidogenic cell lines permanently overexpressing the FSHR exist so far (Casarini et al., 2018; Revankar et al., 2004). Other FSHR functions have been reported to be mediated by Gαi and Gαq proteins, the Gβγ dimer (Gloaguen et al., 2011; Ulloa-Aguirre et al., 2018), and other molecules inducing proliferative signals under low FSHR density in the cell membrane (Tranchant et al., 2011). FSHR-mediated activation of protein kinase B (AKT) occurs downstream of G protein activation (Gonzalez-Robayna et al., 2000; Sayers and Hanyaloglu, 2018) and results in

[1]Unit of Endocrinology, Department of Biomedical, Metabolic and Neural Sciences, University of Modena and Reggio Emilia, Ospedale Civile Sant'Agostino-Estense, Via P. Giardini 1355, 41126 Modena, Italy

[2]Center for Genomic Research, University of Modena and Reggio Emilia, Modena, Italy

[3]International PhD School in Clinical and Experimental Medicine (CEM), University of Modena and Reggio Emilia, Modena, Italy

[4]Histology and Embryology Section, Department of Biomedicine and Prevention, University of Rome Tor Vergata, Rome, Italy

[5]Institute of Reproductive and Developmental Biology, Imperial College London, London, UK

[6]Department of Biochemistry and Molecular Biology, Medical University of Lublin, Lublin, Poland

[7]Postgraduate School of Molecular Medicine, Warsaw, Poland

[8]Unit of Endocrinology, Department of Medical Specialties, Azienda Ospedaliero-Universitaria di Modena, Modena, Italy

[9]Department of Medicine and Surgery, Unit of Neurosciences, University of Parma, Parma, Italy

[10]Mother-Infant Department, University of Modena and Reggio Emilia, Modena, Italy

[11]Clinica EUGIN, Modena, Italy

Continued

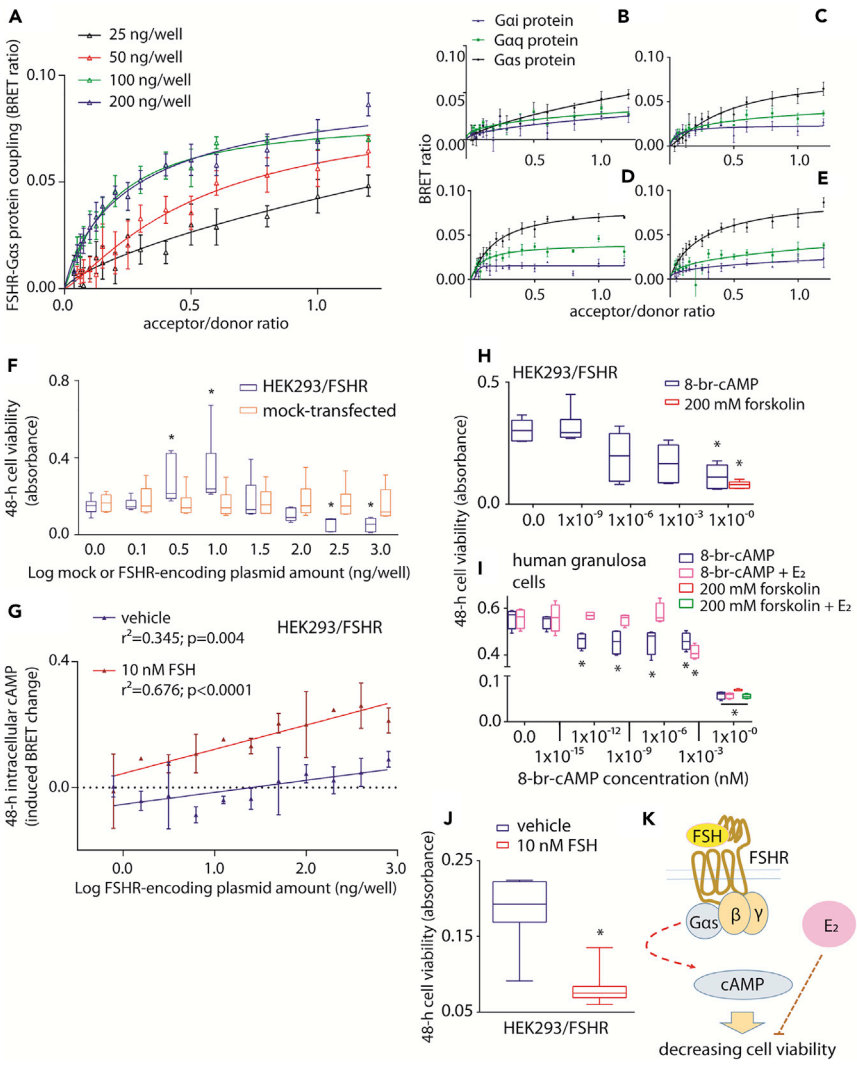

Figure 1. Excessive FSHR Expression Levels Negatively Impact HEK293 Cell Viability

(A) Association of FSHR to the Gαs protein increases with higher receptor expression levels was assessed in HEK293 cells co-expressing the FSHR/rluc- (donor) and the Gαs protein/venus-tagged BRET biosensor. Data were interpolated by non-linear regression and compared by Kruskal Wallis test and Dunn's post-test (100 and 200 ng/well of FSHR-encoding plasmid versus the 25 ng/well condition; $p = 0.0014$; mean ± SEM; $n = 5$).

(B–E) Comparison of constitutive FSHR coupling to Gαs, Gαq, and Gαi with increasing receptor expression levels, in HEK293 cells transfected using 25 (B), 50 (C), 100 (D), and 200 (E) ng/well of FSHR/rluc-encoding plasmid. Receptor level-dependent increase in affinity occurs with Gαs but not with Gαq and Gαi proteins (Kruskal Wallis test and Dunn's post-test; $p < 0.0001$; mean ± SEM; $n = 5$).

(F) Transfected HEK293 cell viability increases at low FSHR-encoding plasmid amounts, whereas decreases at high plasmid concentration. Data were represented by box and whiskers plots (* = significantly different versus coupled mock-transfected sample; Kruskal Wallis test and Dunn's post-test; $p < 0.05$; $n = 6$)

(G) Basal and FSH-induced intracellular cAMP levels with increasing FSHR expression levels. Data are represented as mean ± SEM and interpolated by linear regression ($n = 4$).

(H) Colorimetric assay reveals the relationship between increasing intracellular cAMP concentration and decreasing of HEK293/FSHR cell viability. Cells were treated with increasing concentrations of 8-br-cAMP or 200 mM forskolin (* = significantly different versus 0.0 8-br-cAMP-treated samples; Kruskal Wallis test and Dunn's post-test; $p = 0.0019$).

(I) In human primary granulosa lutein cells, 50 pg/ml E_2 co-treatment inhibits the decrease in cell viability induced by the cAMP analog (* = significantly different versus 0.0 8-br-cAMP-treated samples; Kruskal Wallis test and Dunn's post-test; $p < 0.05$; $n = 8$).

[12]PRC, INRAE, CNRS, IFCE, Université de Tours, Nouzilly, France

[13]Department of Obstetrics and Gynaecology, Fertility Center, ASMN. Azienda Unità Sanitaria Locale – IRCCS di Reggio Emilia, Reggio Emilia, Modena, Italy

[14]Global Medical Affair, Merck KGaA, Darmstadt, Germany

[15]Medical Affair, Merck Serono SpA, Rome, Italy

[16]Department of Life Sciences, University of Modena and Reggio Emilia, Modena, Italy

[17]Center for Neuroscience and Neurotechnology, University of Modena and Reggio Emilia, Modena, Italy

[18]Lead contact

*Correspondence: livio.casarini@unimore.it

https://doi.org/10.1016/j.isci.2020.101812

Figure 1. *Continued*
(J) Cell viability is lower in HEK293/FSHR transfected cells stimulated with FSH compared with vehicle (Mann-Whitney's U-test; p = 0.0003; n = 8).
(K) Summary: FSHR coupling to the Gαs protein/cAMP-pathway, occurring at high receptor expression levels and in the absence of E_2, decreases cell viability. This action is counteracted by estrogen.

anti-apoptotic and proliferative activity in FSHR-expressing ovarian (Rossi et al., 2017) and cancer (Chen et al., 2016) cells.

Estrogens activate two nuclear receptors, ERα and ERβ, and a membrane G-protein-coupled receptor (GPCR), named GPER, mediating rapid E_2-induced intracellular responses such as calcium ion (Ca^{2+} mobilization (Revankar et al., 2005; Thomas et al., 2005)) and found in ovarian tissues throughout the follicular phase (Heublein et al., 2012). Although GPER is coupled to Gαs, it is unable to trigger intracellular cAMP accumulation in response to E_2 in a number of cell models (Broselid et al., 2014). This is due to the interaction of GPER with both the membrane-associated guanylate kinases (MAGUK) and protein-kinase-A-anchoring protein 5 (AKAP5), constitutively inhibiting cAMP in a Gαi/o-independent manner (Broselid et al., 2014). However, opposite data demonstrating that the receptor may trigger cAMP activation were also provided in certain cell models (Filardo et al., 2007; Thomas et al., 2005), suggesting the existence of cell- or culture-specific mechanisms regulating GPER mode of action. GPER mediates survival/proliferation signals through phosphoinositide 3 (PI3K)/phospho-AKT (pAKT) and phospho-extracellular-regulated kinases 1 and 2 (pERK1/2) activation (Gonzalez de Valdivia et al., 2017), as well as Gβγ-dependent mechanisms upregulating proto-oncogenes (Maggiolini et al., 2004).

Ovarian granulosa cells express both FSHR and GPER (Prossnitz and Maggiolini, 2009) modulating a network of proliferative signals (Heublein et al., 2013; Pavlik et al., 2011) fundamental for regulating gametogenesis (Heublein et al., 2012). Consistent with its impact on cell growth, FSHR expression was found in pathological contexts characterized by uncontrolled cell proliferation, such as tumors (Choi et al., 2004) or endometriosis (Ponikwicka-Tyszko et al., 2016), suggesting that it could be a target for still outstanding anti-cancer therapies (Perales-Puchalt et al., 2019). Similarly, GPER expression has been described in several tumor cells (Filardo, 2018), including breast, endometrium, and ovary (Barton et al., 2018), where it may cooperate with FSHR in inducing uncontrolled cell proliferation (Heublein et al., 2013; Li et al., 2007).

Physiologically, high FSHR expression occurs transitorily in the ovarian granulosa cells, decreasing once a single dominant follicle is selected (Jeppesen et al., 2012). We reasoned that the opposing nature of FSHR activity, proliferative and pro-apoptotic, may rely on the cooperation with other factors modulating FSHR signaling. In particular, as described for other structurally similar GPCRs (Guitart et al., 2019; Ji et al., 2004; Jonas et al., 2018; Rivero-Müller et al., 2010), FSHR signaling may be regulated by forming heteromers with other receptors (Casarini et al., 2018). Here, we demonstrate that GPER and FSHR interactions reprogram FSHR-related death into life signals, upregulating the viability of FSHR-/GPER-expressing cells including human ovarian granulosa cells. Together, our data provide a mechanistic model for dominant follicle selection in humans and a novel therapeutic target for poor FSH-responder women undergoing controlled ovarian stimulation.

RESULTS

FSH and cAMP Pro-apoptotic Potential Is Associated with FSHR Expression Levels and Is Counteracted by E_2

We first evaluated the FSHR-related potential of activating steroidogenic and pro-apoptotic signals, likely associated with cAMP production (Aharoni et al., 1995; Casarini and Crépieux, 2019). Intracellular accumulation of cAMP depends on FSHR-Gαs protein coupling, which constitutively increases together with receptor expression levels (Tubio et al., 2010). This was demonstrated by employing Gαs- and FSHR-tagged BRET biosensors, which resulted in left-shifted BRET saturation curves at the maximal concentration of receptor-encoding plasmid used to transfect HEK293 (HEK293/FSHR) cells. This indicates a greater receptor-G protein association affinity is achieved when FSHR is highly expressed (Figures 1A and S1). The receptor expression-dependent association with Gαs was not observed with other G proteins reported to be FSHR intracellular interactors, such as Gαi and Gαq (Figures 1B–1E, S2 and S3). Although Gαs likely competes with other interactors for binding a low number of FSHRs, the potential of decreasing cell viability

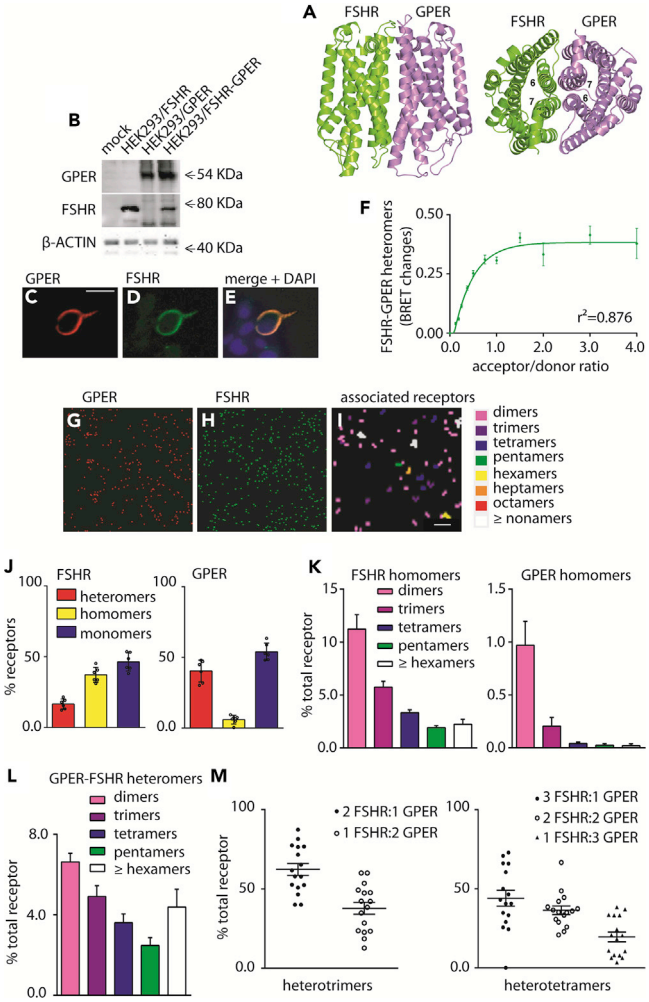

Figure 2. The FSHR Forms Heteromers with GPER

(A) Predicted structural model of the heterodimer between FSHR (green) and GPER (violet) seen in directions perpendicular (left) and parallel (right) to the bundle main axis. In this dimer, H6 of FSHR interacts with H7 of GPER and H6 of GPER interacts with H7 of FSHR.

(B) Western blotting for FSHR and GPER transient expression and co-expression in HEK293 cells, using validated receptor-specific antibodies (Figure S6). β-ACTIN was used as loading control.

(C–E) Representative confocal microscopy image of tagged-GPER and FSHR co-localization by immunofluorescence, in HEK293 cells transiently transfected with FSHR and GPER. A specific primary antibody was used for GPER followed by a TRITC-labelled secondary antibody, whereas nuclei were blue-stained by DAPI. FSHR was visualized by the venus tag. Bar = 25 μm.

(F) Formation of FSHR/rluc- and GPER/venus-tagged heteromers in transfected HEK293 cells. BRET ratio values resulting from molecular interactions were represented as mean ± SEM. Specific association is indicated by data interpolation using non-linear regression, which results in BRET saturation curve (n = 4).

(G and H) FSHR-GPER associations at the single-molecule level were visualized and quantitated by photo-activated localization microscopy with photo-activatable dyes (PD-PALM) in HEK293 cells.

(I) Representative reconstructed PD-PALM images of detected FLAG-GPER and HA-FSHR molecule at the plasma membrane. Images are reconstructed from 2-2 μm^2 areas after x-y coordinate localization using QuickPALM followed by a 50 nm radius neighborhood analysis of receptor molecules. Scale bar represents 0.3 μm.

(J) Quantitative analysis of hetero-, homo-, and monomeric forms of FSHR and GPER when concomitantly expressed in HEK 293, using dual channel PD-PALM; mean ± SEM, n = 5.

(K) Quantitative evaluation of the types of FSHR and GPER homomers. Data are expressed as percentage of total receptor forms, including monomers; mean ± SEM, n = 10.

Figure 2. *Continued*
(L) Quantitative analysis of heteromeric assemblies between FSHR and GPER using dual channel PD-PALM reveals diverse heterodimeric complexes; mean ± SEM, n = 8 cells.
(M) Analysis of individual protomer composition within heterotrimers and heterotetramers demonstrates the preferential occurrence of FSHR protomers versus GPER protomers within these individual multimers; mean ± SEM, n = 8.

(Figure 1F) and of mediating both basal and FSH-induced cAMP activation was FSHR concentration dependent (Figure 1G). Increases in intracellular cAMP is deleterious for the viability of FSHR-expressing cells (Casarini et al., 2016). Indeed, treatment of either HEK293/FSHR or human primary granulosa cells with 8-br-cAMP induces reduction of cell viability in a concentration-dependent manner (Figures 1H and 1I). Interestingly, the cAMP-analog-induced decrease of granulosa cell viability was inhibited by 50 pg/ml E_2 (Figure 1I), suggesting possible crosstalk between opposing gonadotropin- and estrogen-mediated intracellular actions. Indeed, in the absence of E_2, FSH treatment induced a decrease of HEK293/FSHR cell viability (Figures 1J and 1K).

FSHR and GPER Form Heteromeric Complexes at the Cell Membrane

In order to define the mechanism linking FSH and GPER/estrogen-mediated intracellular networks, we employed distinct approaches to examine the formation of possible heterodimers/oligomers involving FSHR and GPER at the cell membrane. Investigation at the atomic level relied on a protein-protein docking-based approach, the FiPD-based approach (Casciari et al., 2006; Fanelli et al., 2013) applied to the structural models of the two receptors. The two independent docking runs by using FSHR as a target and GPER as a probe and *vice versa* converged on the same predicted architecture of the heterodimer (Figure 2A), ranked among the best 10 out of 4,000 solutions, and were characterized by good membrane topology. Remarkably, when using FSHR as a target, the predicted docking solution was the best in score (i.e. rank #1) out of 4,000, belonged to the most populated solution cluster, and showed a good membrane topology (MemTop) score (0.578) (see Methods). The FSHR-GPER interface in the predicted heterodimer is characterized by contacts between H6 and H7 from FSHR and H7 and H6 from GPER, respectively (Figure 2A).

Western blotting and immunofluorescent staining of HEK293/FSHR-GPER cells confirmed expression of both untagged receptors in cell lysates (Figure 2B) and their co-localization at the cell surface (Figures 2C–2E). No signals were detected in GPER- and FSHR-negative cells (Figure 2E). The physical interaction between the two receptors was demonstrated by BRET. In transfected HEK293 cells, transiently expressing both FSHR-rluc and venus-tagged GPER (GPER/rluc) biosensors, a BRET saturation curve was observed with increasing acceptor concentration, indicating specific interactions between the two receptors (Figures 2F, S4, and S5). Further evidence of FSHR-GPER heteromer assembly at the plasma membrane was provided by total internal reflection microscopy (TIRF-M) and photo-activated localization microscopy with photoactivatable dyes (PD-PALM) (Figures 2G–2I), a super-resolution imaging approach we have previously employed to quantitate protomer composition within asymmetric heteromer complexes between LHCGR mutants and between FSHR and LHCGR at the plasma membrane (Jonas et al., 2015, 2018). HEK 293 cells expressing HA-tagged FSHR and FLAG-tagged GPER were labeled with CAGE500-conjugated anti-HA and CAGE552-conjugated anti-FLAG antibodies and fixed for PD-PALM with TIRF-M imaging (Figures 2G–2I). Both FSHR and GPER existed as pre-existing monomers, homomers, and heteromers (Figure 2J). Although both receptors formed a similar percentage of monomers, within the associated populations FSHR exhibited a greater number of homomers over heteromers, whereas conversely the predominant associated form for GPER was heteromers with FSHR. Furthermore, FSHR exhibited a range of homomeric complexes (from dimers, to a range of oligomers) similar to our previous reports with LHCGR (Jonas et al., 2015), whereas at a low level compared with all associations, the GPER-GPER complexes that were detected were primarily dimeric (Figure 2K). GPER-FSHR heteromers at the plasma membrane were also observed in cells co-expressing these receptors, consistent with the BRET data. The heteromer population consisted of heterodimers and a range of hetero-oligomeric complexes (Figure 2L). As we have previously demonstrated that receptor complexes >5 protomers are density dependent, whereas low-order oligomers are density independent (Jonas et al., 2015), we focused further analysis of the protomer identity within individual low-order hetero-oligomeric complexes. This revealed such complexes favored formation of FSHR dominant hetero-oligomers (Figure 2M), consistent with the "preference" for this receptor to exhibit diverse oligomeric forms, and also indicates potential asymmetry in these low-order hetero-oligomers. Overall, these data demonstrate that FSHR and GPER preform into distinct heteromeric assemblies at the plasma membrane and that GPER associations are preferentially formed with FSHR than with itself.

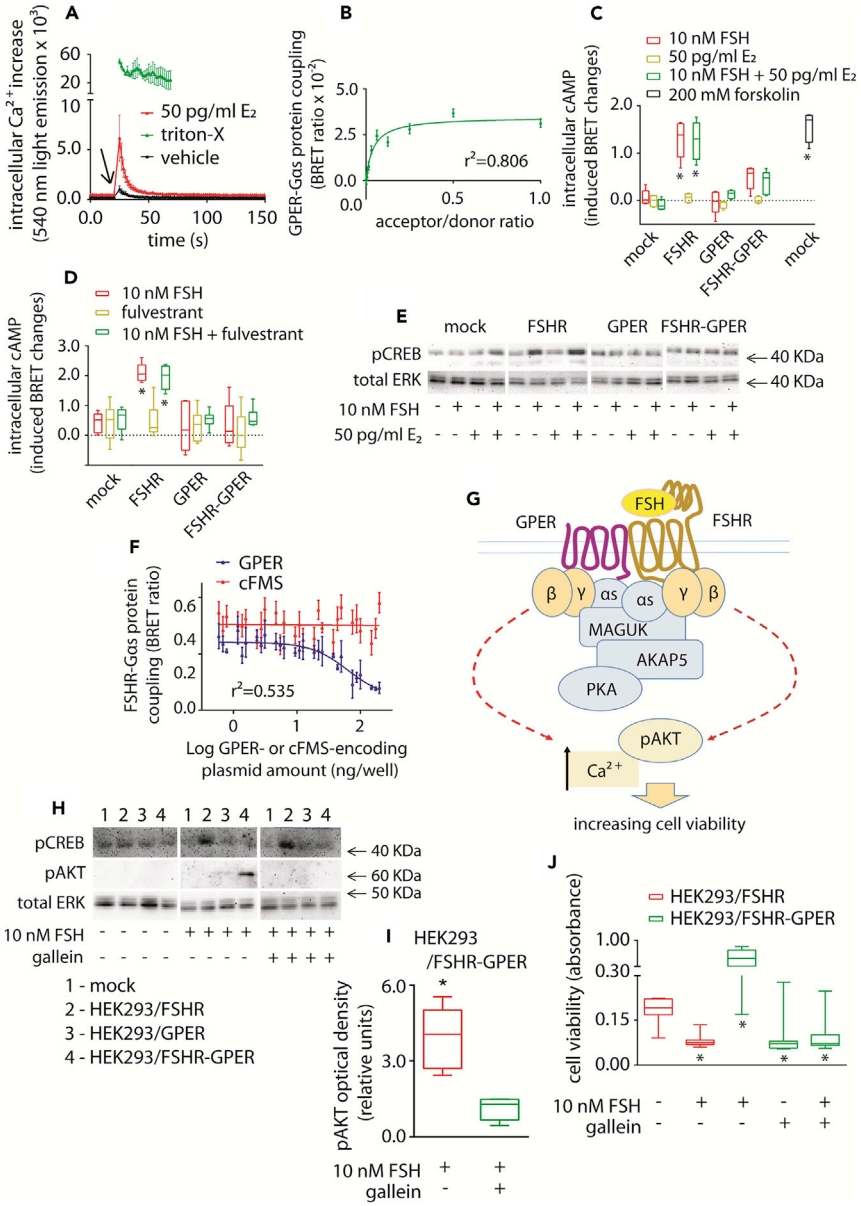

Figure 3. FSHR-GPER Crosstalk Promotes FSH-Stimulated Cell Viability via Gβγ Dimers

(A) GPER transiently expressed in HEK 293 cells simulates E2-induced intracellular Ca^{2+} increase (Kruskal-Wallis test; $p < 0.0001$; n = 8; mean ± SEM). Signals were captured by BRET over 150 s, in the presence of the calcium-biosensor. PBS (vehicle)-treated cells provided basal levels. Cells lysed by Triton X- were positive controls and only a 43-s time window is representatively shown. Compounds were added at the 21-s time point.

(B) GPER/rluc-coupling to the Gαs protein/venus-tagged was demonstrated by BRET. Values are mean ± SEM, and the logarithmic curve was obtained after interpolation using non-linear regression (n = 8).

(C) 10-nM FSH induced cAMP increase in HEK293 cells expressing either one or both FSHR and GPER. 50 pg/ml E2 were added as indicated, whereas mock-transfected and forskolin-treated cells served as basal and positive control, respectively. cAMP values are indicated as induced BRET changes over vehicle-treated mocks (* = significantly different versus FSH-treated mocks; two-way ANOVA with Dunnett's correction for multiple tests; $p < 0.0001$; n = 5; mean ± SEM).

(D) Evaluation of 10-nM FSH-induced intracellular cAMP increase, in the presence and in the absence of the nuclear estrogen receptor blockade by fulvestrant. * = significantly different versus FSH-treated mocks; two-way ANOVA with Dunnett's correction for multiple tests; $p < 0.0001$; n = 5; means ± SEM.

(E) Representative Western blotting analysis of the cAMP-dependent pCREB activation, in HEK293 cells expressing either one or both FSHR and GPER. 50 pg/ml E2 were added where indicated and total ERK served as normalizer.

Figure 3. *Continued*

(F) Decrease of BRET signal indicating a reduced FSHR/rluc-Gαs protein/venus interaction along with increasing untagged GPER expression levels (n = 3; mean ± SEM). The receptor-tyrosine kinase colony-stimulating factor-1 receptor (cFMS) was the negative control.

(G) Proposed model of the FSHR/cAMP signaling blockade by the GPER-associated inhibitory machinery. The MAGUK/AKAP5 complex might physically interact with the Gαs protein coupled to FSHR upon heteromer formation, resulting in cAMP signaling blockade. At this point we hypothesized that FSH-dependent intracellular signals modulating cell viability could be activated by the βγ dimer.

(H) Evaluation of Gαs protein-dependence of pCREB and βγ dimer-dependence of 15-min pAKT activation in HEK293 cells expressing either one or both FSHR and GPER, respectively. The βγ dimer inhibitor gallein was used where indicated and total ERK was the normalizer.

(I) Semi-quantification of the 15-min pAKT signal obtained by western blotting in HEK293/FSHR-GPER cells treated by FSH (* = significantly different versus gallein-treated cells; Mann-Whitney's U-test; $p = 0.002$; n = 6; see Figure S9 for semi-quantification of pAKT signals).

(J) Decreasing of 10 nM FSH-induced cell viability in FSHR-GPER-co-expressing HEK293 cells due to βγ dimer-blockade by gallein. Results were compared with cell viability data from gallein-untreated cells and HEK293/FSHR cells of Figure 1J (cells transfected by 1×10^3 ng/well FSHR-encoding ± 1×10^3 ng/well GPER-encoding plasmid; * = different versus mock; Kruskal-Wallis test; $p < 0.0001$; n = 8; mean ± SEM).

FSH Stimulation of FSHR-GPER Heteromers Promotes Cell Viability via Inhibition of cAMP Signaling

A potential functional association of GPER with FSHR in modulating cell viability was next investigated. HEK293/GPER expressing cells displayed a rapid intracellular Ca^{2+} increase (Figure 3A) occurring immediately upon 50 pg/mL estradiol addition, demonstrating expression of functional GPER (Revankar et al., 2005). BRET measurements also revealed that GPER can couple to Gαs (Figure 3B), although the receptor is unable to mediate cAMP production upon ligand binding (Figure 3C), consistent with previous reports demonstrating the association of GPER with a cAMP/PKA inhibitory complex assembled by MAGUK and AKAP5 proteins (Broselid et al., 2014). Intracellular cAMP levels were maximally stimulated upon FSH treatment of HEK293/FSHR cells but, interestingly, not in HEK293 cells co-expressing FSHR and GPER (Figure 3C), nor in GPER-expressing cells (Figures 3C and S7). These data indicate that the presence of GPER inhibits the increase of intracellular cAMP, independent of the presence or absence of E_2, in FSHR-expressing cells. This effect is specifically targeted to FSHR, because LH treatment of LHCGR-GPER co-expressing HEK293 cells induces an increase in intracellular cAMP to similar levels as in the absence of GPER (Figure S8). Moreover, GPER-dependent inhibition of FSH-induced cAMP signaling occurs even under blockade of the nuclear estrogen receptor by fulvestrant (Figure 3D), thus excluding its involvement. The ability of GPER to inhibit FSH-mediated cAMP signaling was confirmed by measurement of FSH-induced CREB phosphorylation, a downstream cAMP-dependent event (Figure 3E).

To determine if FSHR and Gαs basal coupling was altered in cells co-expressing GPER, FSHR-Gαs coupling was measured via BRET. Increasing levels of GPER decreased BRET signals between FSHR and Gαs (Figures 3F and S8). Although it is unknown whether the decay of the BRET signal corresponds to an uncoupling or structural rearrangement of the FSHR-Gαs complex, it is indicative of a physical perturbation of such complex by GPER. We hypothesized that the GPER/MAGUK/AKAP5 complex associates with FSHR upon heteromer formation perturbing FSHR-Gαs pre-coupling. This disables the ability of FSH to increase cAMP, while not affecting Gβγ-dependent signaling by FSH (Figure 3G). This hypothesis was explored by measuring Gβγ-dependent AKT phosphorylation by FSHR-GPER heteromers, in response to FSH (Figure 3H). Acute FSH treatment (15 min) did not induce pAKT activation in HEK293/FSHR cells, which requires chronic FSH stimulation to detect activation (Nechamen et al., 2007). In contrast, pAKT activation was increased in FSH-treated HEK293/FSHR-GPER cells and was inhibited by the selective Gβγ inhibitor gallein (Figure 3I). GPER also increased cell viability following FSH treatment in FSHR-GPER cells (Figure 3J), compared with HEK293/FSHR cells (Figure 1J), which critically was also inhibited by gallein. Taken together, these results demonstrate that GPER is capable of downregulating FSHR/Gαs/cAMP to increase cell viability via a Gβγ-dependent mechanism.

Disruption of FSHR-GPER Heteromer Formation Results in FSH-Induced Decrease in Cell Viability

To demonstrate that in cells co-expressing FSHR and GPER, FSH/FSHR-mediated increase in cAMP and cell viability was directly due to FSHR-GPER heteromer formation, a mutant GPER (GPER(mut)) was created

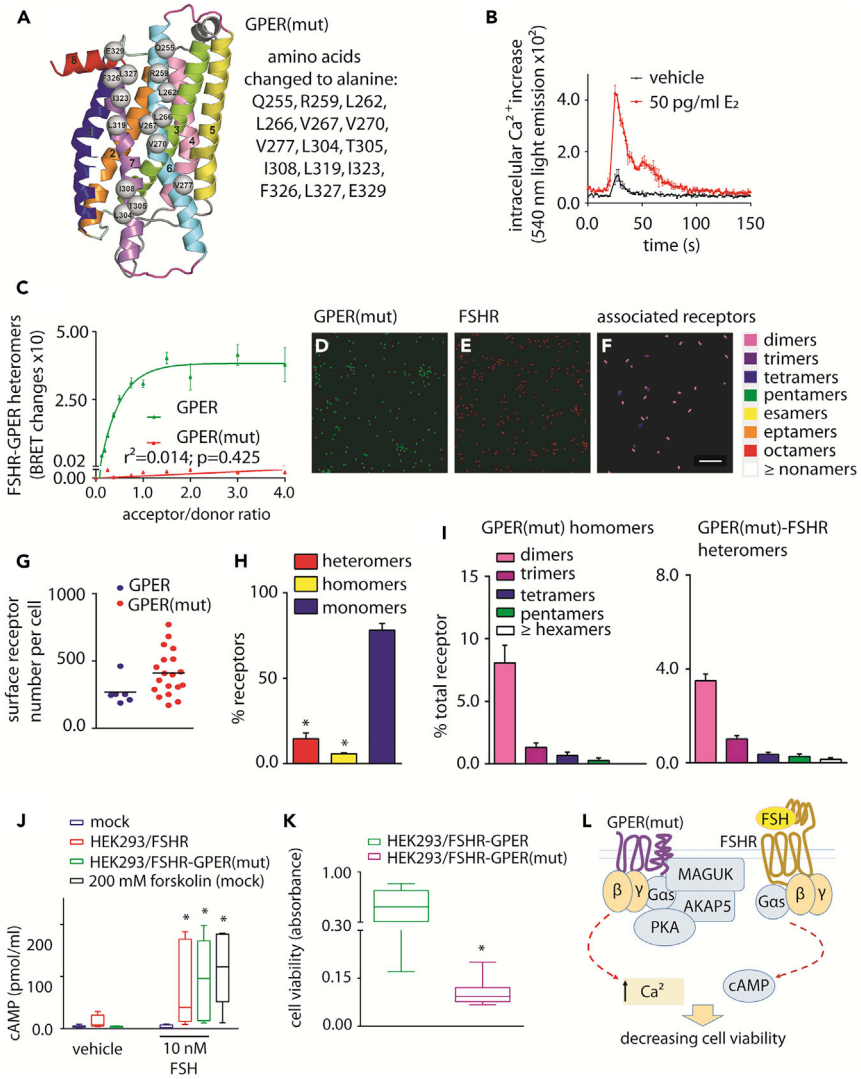

Figure 4. Decrease of Cell Viability by Disruption of FSHR-GPER Heteromers

(A) Side view, in a direction perpendicular to the bundle main axis, of the GPER structural model. The receptor regions are colored as follows: H1, H2, H3, H4, H5, H6, H7, and H8 are, respectively, blue, orange, green, pink, yellow, aquamarine, violet, and red; I1 and E1 are slate; I2 and E2 are gray; and I3 and E3 are magenta. The receptor amino acids participating in the interface with FSHR and subjected to alanine replacement are represented as spheres centered on the Cα-atom. They include Q255, R259, L262, L266, V267, V270, and V277 in H6, L304, T305, I308, L319, I323, and F326, and L327 in H7, and E329 in H8. To obtain a GPER(mut) molecule unable to form heteromers, interacting residues indicated in the box were changed to alanine by *de novo* DNA synthesis.

(B) Demonstration of GPER(mut) functionality by BRET using the calcium-biosensor, in transiently transfected HEK293 cells. The mutant receptor mediates E_2-induced intracellular Ca^{2+} increase compared with vehicle, over 150 s (two-way ANOVA; $p < 0.0001$; $n = 8$; mean ± SEM). Compounds were injected at the 21-s time point.

(C) FSHR/rluc- and GPER(mut)/venus-tagged proteins do not form heteromers. BRET ratio values resulting from molecular interactions are represented as mean ± SEM, together with data from non-mutant GPER (Figure 2F). Specific association is indicated by data interpolation using linear regression ($n = 4$).

(D–I) Confirmation of GPER(mut) membrane localization and lack of heteromerization with FSHR.

(D–F) Representative reconstructed PD-PALM images and heatmap of associations following localization and neighborhood analysis. Scale bar = 0.3 μm

(G) Similar number of GPER and GPER(mut) receptors were expressed at the cell membrane ($p = 0.06$; Mann-Whitney's *U*-test).

(H) Quantitative analysis of hetero-, homo-, and monomeric forms of GPER(mut) when co-expressed with FSHR in HEK293, using dual channel PD-PALM (* = significantly different versus monomers; unpaired t test; $p < 0.0001$; mean ± SEM, $n = 19$).

Figure 4. *Continued*

(I) Quantitative evaluation of the types of GPER(mut) homomers and of heteromeric assemblies with FSHR as a percentage of all receptor forms, including monomers. Mean ± SEM, n = 8 cells.

(J) cAMP increase induced by 10 nM FSH, in HEK293 cells expressing either one or both FSHR and GPER(mut). Mock-transfected and forskolin-treated cells served as basal and positive control, respectively. cAMP values were measured by ELISA and indicated pmol/mL (* = significantly different versus FSH-treated mocks; two-way ANOVA with Tukey's correction for multiple tests; $p \leq 0.0106$; n = 8; mean ± SEM).

(K) Comparison of HEK293/FSHR-GPER (Figure 3J) and HEK293/FSHR-GPER(mut) cell viability, under treatment with 10 nM FSH (* = different versus HEK293/FSHR-GPER; Mann-Whitney's *U*-test; p = 0.0003; n = 8; means ± SEM).

(L) Proposed model showing the inability of GPER(mut) to inhibit the activation of FSH-stimulated cAMP production with ensuing decrease of cell viability due to disruption of heteromerization.

that would not form heteromers with FSHR. To this purpose, the predicted structural model of the heterodimer was exploited to drive site-directed mutagenesis. All the H6 and H7 non-glycine and non-alanine amino acids facing FSHR were replaced by alanines, leading to a GPER form mutated in fifteen positions distributed along the whole length of the two helices, the last amino acid being the beginning of H8 (Figure 4A). GPER(mut) was still able to activate calcium signaling (Figure 4B) but was unable to form heteromers with FSHR as demonstrated by the lack of a saturated BRET signal (Figure 4C). GPER(mut) was expressed at the plasma membrane in cells co-expressing FSHR as detected by PD-PALM (Figures 4D–4F) and was expressed at similar levels to wild-type (WT) GPER (Figures 4G and S10). A dramatic reduction in the number of heteromeric associations occurred (from 40.3% ± 3.1% heteromers for WT GPER to 14.6% ± 3.4% for GPER(mut), Figures 2J and 4H)), while the homomer population which even with WT GPER was not altered (Figure 4H). Unexpectedly, the organization of GPER homomers resulted in an increase in the proportion of homodimers (Figure 4I), compared with WT GPER (Figure 2K), possibly suggesting that distinct homomer interface with a distinct affinity to the heteromer interface and/or mutation of H6-7 results in enhanced stabilization of a homodimer association. Critically, quantitative analysis of individual heteromer complexes revealed that while all forms were decreased, it was primarily formation of the hetero-oligomers that was impeded through mutation of GPER (Figure 4I). In cells co-expressing GPER(mut) and FSHR, 10-nM FSH treatment induced increases in intracellular cAMP (Figure 4J) and decreased cell viability when compared with FSH-treated cells co-expressing wild-type GPER and FSHR (Figure 4K). Therefore, inhibition of FSHR-mediated cAMP signaling and increased cell viability is due to a physical interaction between FSHR and GPER (Figure 4L).

GPER Requires the MAGUK/AKAP5 Complex to Inhibit FSHR-Mediated Decrease in Cell Viability

The role of known GPER-linked machinery (Broselid et al., 2014) in inhibiting FSHR-mediated cAMP response was evaluated in HEK293 cells via a genome editing approach. *AKAP5* was knocked-out in HEK 293 cells by CRISPR/Cas9 (AKAP5-KO HEK293 cells) (Figures 5A, S11, and S12). In these cells, GPER still exhibited heteromer formation with FSHR, as measured by BRET (Figure 5B). However, FSH treatment of AKAP5-KO HEK293 cells, co-expressing GPER and FSHR, induced intracellular cAMP generation (Figure 5C), demonstrating AKAP5 is essential in exerting GPER-dependent inhibition of cAMP production occurring via FSHR. Consistent with the cAMP data, the GPER rescue of cell viability requires AKAP5 (Figure 5D), strengthening the role of this inhibitory machinery in counteracting FSHR activity by GPER. Therefore, one of the molecular mechanisms regulating FSHR-activation of Gαs protein-dependent signals requires the association of GPER and AKAP5, as cells expressing FSHR/GPER, but lacking AKAP5, are able to generate cAMP and thus reduce FSHR-dependent cell viability (Figure 5E).

FSHR and GPER Co-Expression Is Linked to Ovarian Follicle Maturation: In Vivo, Pharmacological Relevance in an Assisted Reproduction Setting

To investigate if FSHR-GPER co-expression may have physiological and clinical relevance, the levels of these receptors at mRNA and protein were evaluated in granulosa cells collected from ovarian follicular fluids of women undergoing FSH stimulation for assisted reproduction techniques (ART). The presence of both FSHR and GPER protein in granulosa cells was demonstrated by immunostaining of human ovarian follicle tissue sections (Figures 6A and 6B) following antibody validation (Figure S6). This was confirmed by Western blotting of human granulosa and transfected HEK293 cell lysates, in the presence and in the absence of *GPER* mRNA depletion by siRNA (Figure 6C), where the anti-FSHR or anti-GPER antibodies produced a signal in cells expressing only these receptors (Figure 6C).

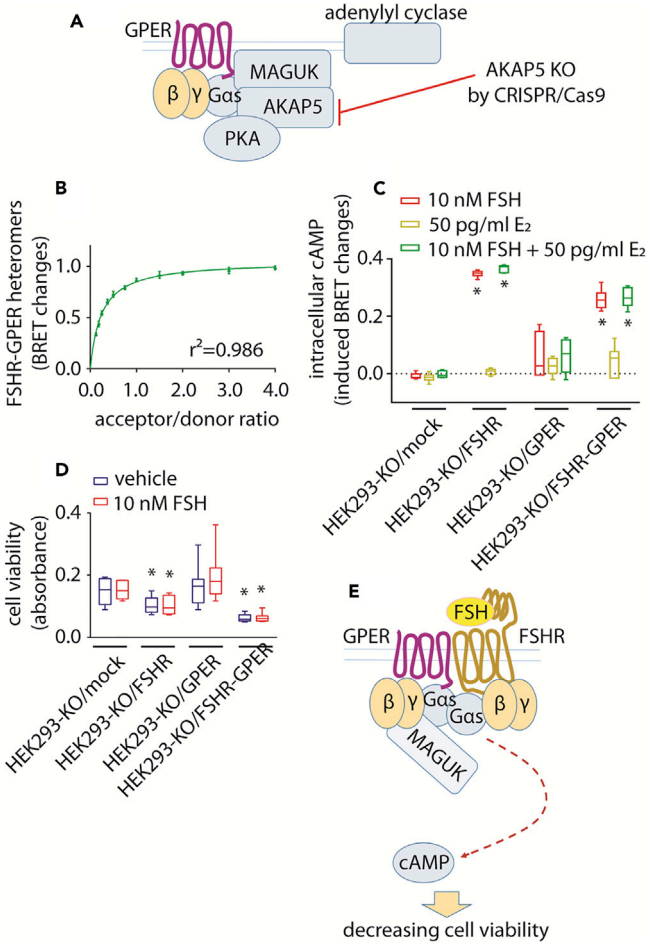

Figure 5. Cell Viability Decreases upon Disrupting the GPER-Associated MAGUK/AKAP5 Molecular Inhibitory Complex

(A) Model depicting the development of the AKAP5-KO HEK293 cell line by CRISPR/Cas9. The absence of AKAP5 leads to disruption of the GPER-associated inhibitory machinery without impairing FSHR-GPER heteromer formation.

(B) FSHR/rluc-GPER/venus-tagged heteromer formation evaluated by BRET, in AKAP5-KO HEK293 cells. Values are expressed as mean ± SEM and interpolated by non-linear regression (n = 4).

(C) Intracellular cAMP increase following 10 nM FSH-treatment of AKAP5-KO HEK293 cells, transiently expressing FSHR and/or GPER. Fifty pg/ml E_2 were added where indicated and signals acquired by BRET. * = significantly different versus FSH-treated mocks; two-way ANOVA with Tukey's post-hoc test; $p < 0.0001$; n = 6; means ± SEM.

(D) Viability of FSHR- and/or GPER-expressing AKAP5-KO HEK293 cells in the presence and in the absence of 10 nM FSH (* = different versus mock; two-way ANOVA with Dunnett's post-hoc test; $p < 0.0001$; n = 8; means ± SEM).

(E) Model describing the failure of the inhibition of FSHR/Gαs protein signaling and cell viability decrease, in the absence of AKAP5.

FSHR/*GPER* mRNA expression levels were matched with clinical parameters indicative of *in vivo* proliferation. A group of 91 women were subdivided into two groups; "normo-responders" were defined as women providing >4 oocytes upon controlled ovarian stimulation, whereas "poor responders" as women providing ≤4 oocytes (Ferraretti et al., 2011; Polyzos and Sunkara, 2015). Granulosa cells from donor women were cultured for one week to enable cells to recover following gonadotropin hyperstimulation during ART procedure and mRNA levels of *FSHR* and *GPER* quantified, plotted in an X-Y graph, and interpolated by non-linear regression. In normo-responder women, *FSHR* expression increased linearly together with *GPER* transcripts (Figures 6D, S13, and S14). The functional importance of such a ratio is supported by the finding that in FSH poor responders, low oocyte yield is correlated to higher *FSHR* over *GPER* expression, suggesting this may impact cell survival.

The role of GPER in counteracting intracellular death signals through crosstalk with FSHR was confirmed using human primary granulosa cells, where the effects of FSH were evaluated in the presence and absence

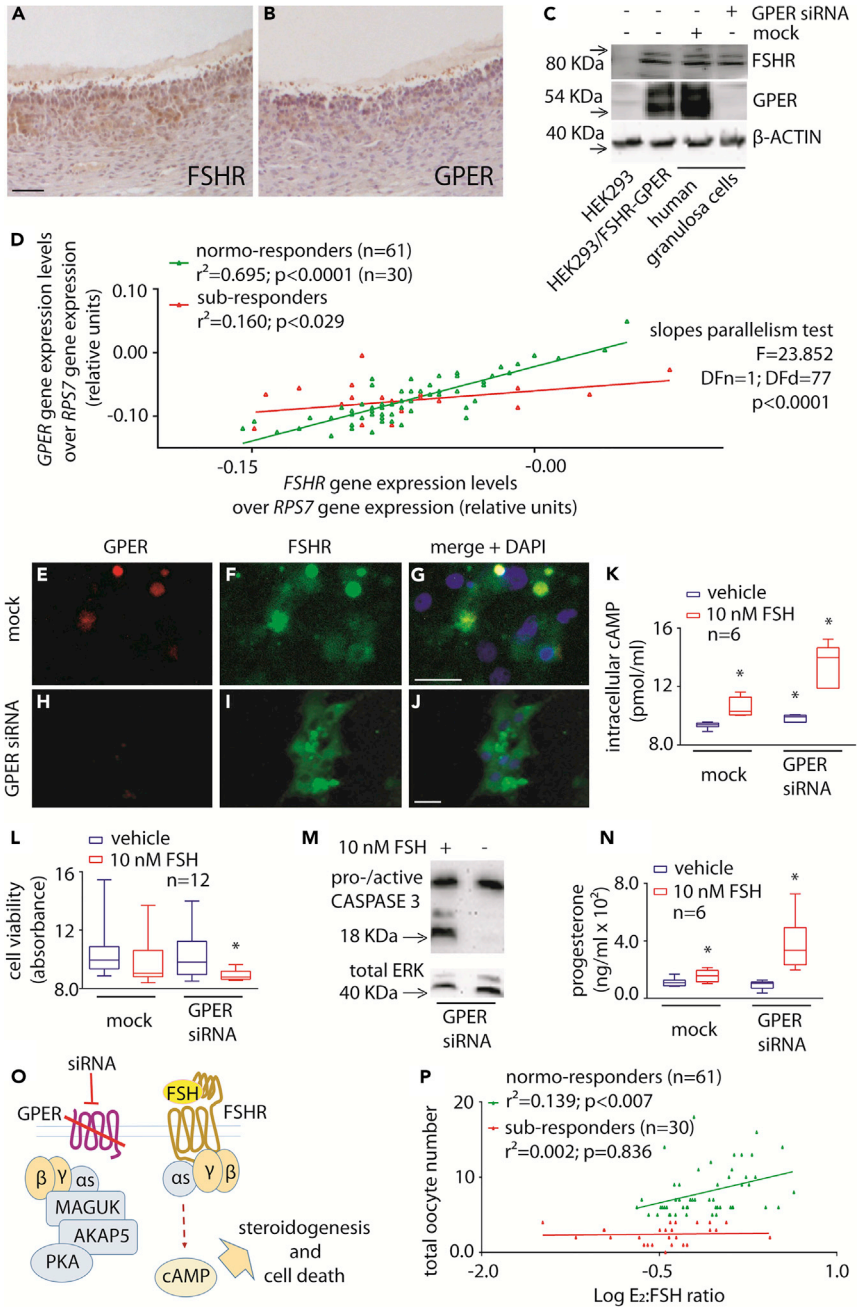

Figure 6. Link Between FSHR-GPER Co-expression and Follicular Growth Response to FSH

(A and B) Representative determination of FSHR and GPER expression in granulosa cells at the antral follicular stage, by immunohistochemistry. Ovarian sections were treated by specific anti-FSHR or -GPER primary antibodies, over hematoxylin background staining (bar = 200 μm).

(C) Western blotting demonstrating the presence of both FSHR and GPER in primary human granulosa cell lysates and the inhibition of expression of GPER by 48-h siRNA. HEK293 transiently transfected with FSHR- and GPER-encoding plasmids were used as controls. The efficacy of GPER siRNA is shown and compared with control siRNA (mock)-treated granulosa cells. β-ACTIN was used as a loading control.

(D) Correlation between *FSHR* and *GPER* gene expression levels in granulosa cells collected from donor normo- (n = 61) and poor-responder (n = 30) women undergoing FSH stimulation for assisted reproduction. Each patient is represented by a point, and mRNA levels were measured by real-time PCR, normalized over the *RPS7* housekeeping gene and interpolated by linear regression. Immunohistochemistry and uncropped western blotting for antibody validation are provided as supplemental materials (Figure S6).

Figure 6. *Continued*

(E–J) Representative images of GPER and FSHR co-localization in 48-h mock- (E-G) and GPER siRNA-treated (H-J) human granulosa cells, detected by immunofluorescence. Specific primary antibody was used for FSHR and GPER binding, as well as TRITC- (E, H) and FITC-labelled (F, I) secondary antibodies, respectively. Nuclei (blue) were stained by DAPI (G, J). Bar = 25 μm.

(K) Intracellular cAMP levels measured in control and GPER siRNA-treated granulosa cells by ELISA, in the presence or absence of 10 nM FSH. Data are represented by box and whiskers plots (* = different versus vehicle/mock-treated cells; two-way ANOVA and Sidak's multiple comparisons test; $p \leq 0.0074$; n = 8).

(L) Granulosa cell viability after 48-h treatment with control/GPER siRNA. Effects of 10-nM FSH were also assessed 24 h before measurements (* = different versus vehicle/mock-treated cells; Kruskal-Wallis with Dunn's correction for multiple tests; p = 0.0002; n = 12).

(M) Evaluation of procaspase 3 cleavage in granulosa cells under 48-h GPER depletion by siRNA. 10-nM FSH was added 24 h before analysis, as indicated, while total ERK was the loading control.

(N) Progesterone levels measured in media of control and GPER siRNA-treated granulosa cells, maintained 24 h in the presence or in the absence of 10 nM FSH, by immunoassay. (* = different versus vehicle/mock-treated cells; two-way ANOVA and Fisher's test; $p \leq 0.001$; n = 6).

(O) Model describing the FSHR/Gαs protein-dependent activation of the steroidogenic/apoptotic pathway, under GPER depletion by siRNA.

(P) Correlation between oocyte number and the ratio between E_2 serum levels and cumulative FSH dose of normo- (n = 61) and poor-responder (n = 30) women. Patients are represented by points, and data were interpolated using linear regression.

of GPER via siRNA (Figures 6C and 6E–6J). These data suggest FSHR-GPER interaction occurring also in hGLC, as confirmed by proximity ligation assay (Figure S15). Interestingly, GPER-depleted granulosa cells exhibited both increased basal and FSH-induced cAMP production, compared with mock-treated cells (Figure 6K), and similar results were obtained in AKAP5 siRNA-treated cells (Figure S16). Moreover, 10-nM FSH treatment reduced cell viability following GPER depletion (Figure 6L) and induced procaspase 3 cleavage as detected by Western blotting (Figure 6M), suggesting the protective role of GPER from gonadotropin-induced cell death. In these experiments, all samples were maintained under LHCGR depletion via siRNA, as LHCGR has been reported to negatively regulate cAMP signaling from FSHR via LHCGR/FSHR heteromers (Feng et al., 2013). As increases in intracellular cAMP (Figure 6K) is known to drive steroid synthesis in granulosa cells, the amount of progesterone secreted in FSH-treated cells was also significantly increased in human granulosa cells depleted of GPER (Figure 6N), thus supporting previously proposed links between steroidogenic and pro-apoptotic pathways in ovarian cells (Amsterdam et al., 2003; Breckwoldt et al., 1996).

These data strongly support a functional requirement of FSHR-GPER associations in the ovary. As we have shown that proportional amounts of both receptor transcripts correlate with high oocyte yield (Figure 6D), in FSH poor responders, low oocyte number is correlated to higher *FSHR* over *GPER* expression, presumably resulting in deleterious FSHR/cAMP-dependent effects for cell survival (Figure 6O). The concept is further assessed by plotting biochemical parameters against the number of oocytes achieving maturation after controlled ovarian stimulation procedures (Figure 6P). The ratio between estradiol levels and cumulative FSH dose, assumed to be indicative of the steroid capability to inhibit the selective pressure *via* activation of proliferative and anti-apoptotic signals in growing oocytes, are correlated in normo-responder women, whereas they are not in poor responders who have lower levels of GPER (Figure 6P). These data further support our findings in human granulosa cells, whereby the reduction of GPER results in enhanced FSH-mediated steroidogenesis but increased loss of cell viability and subsequent decrease in oocyte yield in these patients.

DISCUSSION

This work demonstrates that GPER heteromerization with FSHR shifts the preferential signal transduction from cAMP to pAKT activation, reducing cAMP-dependent apoptosis and favoring cell survival. Our results demonstrate novel aspects of FSHR function, by extending the number of transmembrane partners of FSHR to steroid hormone GPCRs. We also identify the mechanism underpinning GPER-FSHR heteromer inhibition of cAMP signaling is via the GPER-associated MAGUK-AKAP5 protein complex. Critically, our data demonstrate important implications for ovarian physiology and FSH use in fertility treatment, identifying for the first time that FSHR-GPER heteromer represent a druggable target to regulate cell death and survival and improve fertility outcomes in poor FSH responders.

The ability of FSHR-GPER to form heteromers was demonstrated complementarily using different approaches and, interestingly, revealed that GPER formed minimal homomeric associations and preferential formation with FSHR in complexes containing a higher number of FSHR than GPER molecules. In that respect, as FSH is thought to bind and activate FSHR trimers (Jiang et al., 2014), our data could support a role for these asymmetric lower order hetero-oligomers in regulating cell viability. This inhibitory role of GPER on cAMP is specific to FSHR, because GPER had no effect on LHCGR-mediated cAMP, reflecting structural differences between FSHR and LHCGR, in line with the different and specific physiological role of LH (Casarini et al., 2012, 2017). Moreover, it is worth of note that LHCGR-mediated cAMP increase is not linked to cell death, likely due to anti-apoptotic pathways simultaneously activated by the ligand (Casarini et al., 2012, 2016, 2017). Upon FSHR and GPER co-expression, disruption or structural rearrangements of the FSHR-Gαs protein interaction occurs. These rearrangements are GPER dependent and negatively impact the FSH-induced cAMP production via the GPER-related anchoring complex *AKAP5* (Broselid et al., 2014). Data were confirmed in FSHR-GPER co-expressing human primary granulosa cells, where siRNA knockdown of native GPER expression enhanced the FSHR-mediated cAMP steroidogenic pathway (Broselid et al., 2014) and negatively impacted cell viability. Although our data support the lack of E_2-induced cAMP increase via GPER, opposite findings were also obtained (Filardo et al., 2007; Thomas et al., 2005). We could speculate that GPER-mediated cAMP increase could depend on specific conditions, such as the cell type, MAGUK/AKAP5 expression levels, or the type of estrogen binding the receptor. Intact FSHR-GPER complexes responded to FSH treatment by stimulating acute βγ-dependent pAKT activation, which has been associated with cell migration and proliferative events in several cell models (Kamal et al., 2014; Matoba et al., 2018; Ouelaa-Benslama et al., 2012; Surve et al., 2014), and were proposed as a target for tumor-suppressing therapies (Cantley and Neel, 1999). We found this FSHR-associated pAKT activation occurs relatively rapidly upon cell treatment by FSH, in contrast to what has been previously described (Gloaguen et al., 2011). Overall, our findings fulfill the recently proposed criteria for demonstrating functional GPCR heteromers in native tissue: (a) receptor co-localization/interaction, (b) exhibition of distinct functional properties by heteromers compared with protomers, and (c) loss of heteromer-specific properties upon heteromer disruption (Gomes et al., 2016); in our study this was via knockdown of GPER in primary human granulosa cells; equivalent findings were observed with the GPER(mut) that identified TM6-7 as the heteromer interface that when mutated could specifically disrupt interactions with FSHR. To date, these criteria have only been fulfilled by a small subset of family A GPCR heteromers (Gomes et al., 2016). Intriguingly, GPER(mut) homodimers were more prevalent compared with WT GPER, perhaps suggesting a distinct homodimer interface that exhibits a distinct affinity compared with the heteromer TM6-7 interface with FSHR, and/or the GPER(mut) perhaps stabilizes a receptor conformation that results in more stable homomer associations. It is important to note, however, that this mutation, even with altered homomeric associations, did not alter the ability of GPER to activate estradiol-induced calcium signaling.

Although proliferative and anti-apoptotic signals are preferentially activated at relatively low FSHR levels (Tranchant et al., 2011), the steroidogenic/pro-apoptotic pathway is stimulated in the presence of increasing receptor number. This is due to concentration-dependent variations of FSHR association affinity with its different intracellular effectors, as shown for other GPCRs (Bates et al., 2006), which is similar across different G proteins at low receptor expression levels, whereas preferential coupling to Gαs protein and activation of cAMP signaling occurs at high receptor expression levels (Tranchant et al., 2011). In addition, the findings in this study suggest this is likely due to a higher level of FSHR monomers/homomers over FSHR-GPER heteromers. A greater proportion of FSHR only complexes would thus program the cell fate toward FSHR/cAMP-dependent death, a finding well described in the literature (Aharoni et al., 1995; Amsterdam et al., 1998; Breckwoldt et al., 1996; Casarini et al., 2016; Maillet et al., 2002; Sasson et al., 2003; Sirotkin et al., 2008, 2018; Tajima et al., 2002) but neglected for a long-time due to the lack of evidence on the pro-apoptotic action of FSH *in vivo*. Indeed, FSH action is commonly associated with proliferative events, follicular growth being the physiological example, and as suggested by the presence of FSHR in pathological contexts, characterized by uncontrolled cell growth, such as cancer (Choi et al., 2004) or endometriosis (Ponikwicka-Tyszko et al., 2016), which indicated FSHR as a target of anti-cancer drugs (Perales-Puchalt et al., 2019).

The proliferative role of FSH is well known, and indeed this hormone is used as a drug for inducing controlled ovarian stimulation and in the clinical setting of infertility treatment (Behre, 2019; Santi et al., 2018). On the other hand, the physiological FSH action is directed to estrogen biosynthesis, enhancing cell growth *in vivo* (Wallach et al., 1996), and it is not surprising that both hormones are placed within

proliferative contexts. We suggest that the formation of FSHR-GPER heteromers may be involved in the endocrine regulation of ovarian physiology (Hillier, 1994), providing a molecular mechanism explaining why one follicle becomes dominant although it is exposed to the same hormonal *milieu* of other follicles becoming atretic. Accordingly, FSHR-GPER heteromers would support dominance and further growth, whereas the lack/insufficiency of GPER expression, and thus GPER-FSHR heteromers, would direct FSH action toward apoptosis in the follicles, which become atretic. Conversely, GPER KO mice feature pathological conditions such as altered glucose and lipid metabolism (Sharma and Prossnitz, 2016) and tumorigenesis (Marjon et al., 2014), without any specific reproductive phenotype (Prossnitz and Hathaway, 2015). However, the mouse is a multiovulatory species, and species-specific mechanisms underlying the endocrine regulation of multi- versus mono-ovulation are different (Driancourt et al., 1991; Webb et al., 2016). Whether FSHR-GPER heteromerization results from the evolution in mono-ovulatory mammals is a topic of future studies.

The ability of these heteromers to modulate opposing apoptotic and proliferative pathways could have implications in hormone-dependent cancers. A number of pro-apoptotic or anti-proliferative actions have been previously associated with FSHR function (Casarini and Crépieux, 2019; Casarini et al., 2016), especially in conditions of high receptor expression levels, similar to other GPCRs (Revankar et al., 2004). Our data support a mechanism by which FSHR-GPER heteromeric complexes occur and function in certain receptor-expressing tumor cells (Heublein et al., 2013), inhibiting the pro-apoptotic, cAMP pathway and enhancing the activation of proliferative signals by FSH, thereby upregulating tumor growth. A similar mechanism was previously described for other GPCRs (Moreno et al., 2014; Rozenfeld et al., 2011). Patients affected by ovarian carcinoma co-expressing FSHR and GPER have lower prognosis than those with cancer cells expressing FSHR or GPER alone (Heublein et al., 2013). FSHR-GPER heteromerization should be investigated in tumor tissues expressing both receptors, thus representing a potential target for specific drug design. The structural model of the FSHR-GPER interaction predicted and supported by the ability to disrupt the proposed interface at H6-7 may provide a rationale for future structure-based drug design/discovery.

In terms of clinical applications, our study provides evidence for the potential application of these results in improving outcomes in assisted reproduction and infertility treatment. The possibility to boost follicular growth and maturation in women who are poor responders to ovarian stimulation with FSH (e.g. due to advanced age) is a current challenge in reproductive medicine. Novel biologicals could be designed to specifically and transitorily favor FSHR-GPER oligomerization and, thereby, follicular growth and rescue. Indeed, our data suggest that women who are poor responders to FSH stimulation in an assisted reproduction program exhibit low expression of GPER that is not correlated with FSHR expression, possibly reflecting reduced ability to form heteromers and thus an insufficient pro-proliferative FSH action in such conditions.

In summary, we have demonstrated that GPER shifts the pro-apoptotic effects of high FSHR expression levels toward upregulation of cell viability. This occurs via formation of heteromeric complexes capable of inhibiting the cAMP pathway but stimulating pAKT, deviating FSHR coupling from $G\alpha s$ to $G\beta\gamma$. Our data provide a novel and promising target for improving both infertility treatment and cancer therapy, through the development of drugs favoring or inhibiting FSHR-GPER heteromer function, respectively.

Limitations of the Study

Although gene expression data in granulosa-luteal cells from women undergoing ART were provided, this is an *in vitro*-based study and receptor-receptor heteromer formation would need further evaluation in ovarian follicles of different developmental stages.

Resource Availability

Lead Contact

Further information and requests for resources and reagents should be directed to and will be fulfilled by the lead contact, Livio Casarini: livio.casarini@unimore.it.

Materials Availability

All unique/stable reagents generated in this study are available from the Lead Contact with a completed Materials Transfer Agreement.

Data and Code Availability

Data that support the findings of this study are available from the Lead Contact on reasonable request.

METHODS

All methods can be found in the accompanying Transparent Methods supplemental file.

SUPPLEMENTAL INFORMATION

Supplemental Information can be found online at https://doi.org/10.1016/j.isci.2020.101812.

ACKNOWLEDGMENTS

This study was supported by the Italian Ministry of University and Research (MIUR). M.S. is an LE STUDIUM RESEARCH FELLOW, Loire Valley Institute for Advanced Studies, Orléans & Tours, France, - INRA - Center Val de Loire, 37380 Nouzilly, France, receiving funding from the European Union's Horizon 2020 research and innovation program under the Marie Skłodowska-Curie grant agreement No 665790. We would like to thank Dr Andreas Bruckbauer at the Facility for Imaging of Light Microscopy (FILM), Imperial College London, for technical support with PALM. A.C.H. was supported by grants from the BBSRC (BB/1008004/1) and Genesis Research Trust, N.S.S is supported by an Imperial College London President's Scholarship. Grant "Departments of Excellence Program" from MIUR to the Department of Biomedical, Metabolic and Neural Sciences (University of Modena and Reggio Emilia). Polish National Science Centre (NCN) grants: DEC-2015/17/B/NZ1/01777, DEC-2017/25/B/NZ4/02364.

AUTHOR CONTRIBUTIONS

LC designed the study, managed experiments, performed data analysis and interpretation, and wrote the manuscript. CL, EP, SL, and LR performed BRET and western blotting experiments and data analysis. SS, and BM performed BRET and gene expression analysis. SM did immunostainings. CA performed gene expression analysis. NSS have applied the PALM method. JC created the CRISP/Cas9-modified cells. GB, FP, ALM, and MTV provided scientific support, primary cells and tissues, and manuscript editing. ML and GO provided scientific support, data interpretation, and manuscript editing. FGK was involved in the management of immunostainings and manuscript editing. FF did bioinformatics analyzes, data interpretation, and manuscript editing. ARM managed CRISPR/Cas9 experiments, supported data analysis, and did manuscript editing. ACH supported experiments and study design, provided data interpretation, scientific support, and manuscript writing. MS provided study and scientific management, data interpretation, and manuscript writing.

DECLARATION OF INTERESTS

ML and GO are Merck Serono SpA employees without any conflict of interest.

Received: June 15, 2020
Revised: October 25, 2020
Accepted: November 11, 2020
Published: December 18, 2020

REFERENCES

Aharoni, D., Dantes, A., Oren, M., and Amsterdam, A. (1995). cAMP-mediated signals as determinants for apoptosis in primary granulosa cells. Exp. Cell Res. *218*, 271–282.

Amsterdam, A., Dantes, A., Hosokawa, K., Schere-Levy, C.P., Kotsuji, F., and Aharoni, D. (1998). Steroid regulation during apoptosis of ovarian follicular cells. Steroids *63*, 314–318.

Amsterdam, A., Sasson, R., Keren-Tal, I., Aharoni, D., Dantes, A., Rimon, E., Land, A., Cohen, T., Dor, Y., and Hirsh, L. (2003). Alternative pathways of ovarian apoptosis: death for life. Biochem. Pharmacol. *66*, 1355–1362.

Barton, M., Filardo, E.J., Lolait, S.J., Thomas, P., Maggiolini, M., and Prossnitz, E.R. (2018). Twenty years of the G protein-coupled estrogen receptor GPER: historical and personal perspectives. J. Steroid Biochem. Mol. Biol. *176*, 4–15.

Bates, B., Zhang, L., Nawoschik, S., Kodangattil, S., Tseng, E., Kopsco, D., Kramer, A., Shan, Q., Taylor, N., Johnson, J., et al. (2006). Characterization of Gpr101 expression and G-protein coupling selectivity. Brain Res. *1087*, 1–14.

Behre, H.M. (2019). Clinical use of FSH in male infertility. Front. Endocrinol. (Lausanne). *10*, 322.

Breckwoldt, M., Selvaraj, N., Aharoni, D., Barash, A., Segal, I., Insler, V., and Amsterdam, A. (1996). Expression of Ad4-BP/cytochrome P450 side chain cleavage enzyme and induction of cell death in long-term cultures of human granulosa cells. Mol. Hum. Reprod. *2*, 391–400.

Broselid, S., Berg, K.A., Chavera, T.A., Kahn, R., Clarke, W.P., Olde, B., and Leeb-Lundberg, L.M.F. (2014). G protein-coupled receptor 30 (GPR30) forms a plasma membrane complex with membrane-associated guanylate kinases (MAGUKs) and protein kinase A-anchoring protein 5

(AKAP5) that constitutively inhibits cAMP production. J. Biol. Chem. *289*, 22117–22127.

Cantley, L.C., and Neel, B.G. (1999). New insights into tumor suppression: PTEN suppresses tumor formation by restraining the phosphoinositide 3-kinase/AKT pathway. Proc. Natl. Acad. Sci. U. S. A. *96*, 4240–4245.

Casarini, L., and Crépieux, P. (2019). Molecular mechanisms of action of FSH. Front. Endocrinol. (Lausanne). *10*, 305.

Casarini, L., Lispi, M., Longobardi, S., Milosa, F., La Marca, A., Tagliasacchi, D., Pignatti, E., and Simoni, M. (2012). LH and hCG action on the same receptor results in quantitatively and qualitatively different intracellular signalling. PLoS One *7*, e46682.

Casarini, L., Reiter, E., and Simoni, M. (2016). β-arrestins regulate gonadotropin receptor-mediated cell proliferation and apoptosis by controlling different FSHR or LHCGR intracellular signaling in the hGL5 cell line. Mol. Cell. Endocrinol. *437*, 11–21.

Casarini, L., Riccetti, L., De Pascali, F., Gilioli, L., Marino, M., Vecchi, E., Morini, D., Nicoli, A., La Sala, G.B., and Simoni, M. (2017). Estrogen modulates specific life and death signals induced by LH and hCG in human primary granulosa cells in vitro. Int. J. Mol. Sci. *18*, 926.

Casarini, L., Santi, D., Simoni, M., and Potì, F. (2018). "Spare" luteinizing hormone receptors: facts and fiction. Trends Endocrinol. Metab. *29*, 208–217.

Casciari, D., Seeber, M., and Fanelli, F. (2006). Quaternary structure predictions of transmembrane proteins starting from the monomer: a docking-based approach. BMC Bioinformatics *7*, 340.

Chen, J., Bai, M., Ning, C., Xie, B., Zhang, J., Liao, H., Xiong, J., Tao, X., Yan, D., Xi, X., et al. (2016). Gankyrin facilitates follicle-stimulating hormone-driven ovarian cancer cell proliferation through the PI3K/AKT/HIF-1α/cyclin D1 pathway. Oncogene *35*, 2506–2517.

Choi, J.-H., Choi, K.-C., Auersperg, N., and Leung, P.C.K. (2004). Overexpression of follicle-stimulating hormone receptor activates oncogenic pathways in preneoplastic ovarian surface epithelial cells. J. Clin. Endocrinol. Metab. *89*, 5508–5516.

Correia, S., Cardoso, H.J., Cavaco, J.E., and Socorro, S. (2015). Oestrogens as apoptosis regulators in mammalian testis: angels or devils? Expert Rev. Mol. Med. *17*, e2.

Driancourt, M.A., Webb, R., and Fry, R.C. (1991). Does follicular dominance occur in ewes? J. Reprod. Fertil. *93*, 63–70.

Fanelli, F., Seeber, M., Felline, A., Casciari, D., and Raimondi, F. (2013). Quaternary structure predictions and structural communication features of GPCR dimers. Prog. Mol. Biol. Transl. Sci. *117*, 105–142.

Feng, X., Zhang, M., Guan, R., and Segaloff, D.L. (2013). Heterodimerization between the lutropin and follitropin receptors is associated with an attenuation of hormone-dependent signaling. Endocrinology *154*, 3925–3930.

Ferraretti, A.P., La Marca, A., Fauser, B.C.J.M., Tarlatzis, B., Nargund, G., and Gianaroli, L.; ESHRE working group on Poor Ovarian Response Definition (2011). ESHRE consensus on the definition of "poor response" to ovarian stimulation for in vitro fertilization: the Bologna criteria. Hum. Reprod. *26*, 1616–1624.

Filardo, E.J. (2018). A role for G-protein coupled estrogen receptor (GPER) in estrogen-induced carcinogenesis: dysregulated glandular homeostasis, survival and metastasis. J. Steroid Biochem. Mol. Biol. *176*, 38–48.

Filardo, E., Quinn, J., Pang, Y., Graeber, C., Shaw, S., Dong, J., and Thomas, P. (2007). Activation of the novel estrogen receptor G protein-coupled receptor 30 (GPR30) at the plasma membrane. Endocrinology *148*, 3236–3245.

Gloaguen, P., Crépieux, P., Heitzler, D., Poupon, A., and Reiter, E. (2011). Mapping the follicle-stimulating hormone-induced signaling networks. Front. Endocrinol. (Lausanne). *2*, 45.

Gomes, I., Ayoub, M.A., Fujita, W., Jaeger, W.C., Pfleger, K.D.G., and Devi, L.A. (2016). G protein-coupled receptor heteromers. Annu. Rev. Pharmacol. Toxicol. *56*, 403–425.

Gonzalez-Robayna, I.J., Falender, A.E., Ochsner, S., Firestone, G.L., and Richards, J.S. (2000). Follicle-Stimulating hormone (FSH) stimulates phosphorylation and activation of protein kinase B (PKB/Akt) and serum and glucocorticoid-Induced kinase (Sgk): evidence for A kinase-independent signaling by FSH in granulosa cells. Mol. Endocrinol. *14*, 1283–1300.

Gonzalez de Valdivia, E., Broselid, S., Kahn, R., Olde, B., and Leeb-Lundberg, L.M.F. (2017). G protein-coupled estrogen receptor 1 (GPER1)/GPR30 increases ERK1/2 activity through PDZ motif-dependent and -independent mechanisms. J. Biol. Chem. *292*, 9932–9943.

Guitart, X., Moreno, E., Rea, W., Sánchez-Soto, M., Cai, N.-S., Quiroz, C., Kumar, V., Bourque, L., Cortés, A., Canela, E.I., et al. (2019). Biased G protein-independent signaling of dopamine D1-D3 receptor heteromers in the nucleus accumbens. Mol. Neurobiol. *56*, 6756–6769.

Heublein, S., Lenhard, M., Vrekoussis, T., Schoepfer, J., Kuhn, C., Friese, K., Makrigiannakis, A., Mayr, D., and Jeschke, U. (2012). The G-protein-coupled estrogen receptor (GPER) is expressed in normal human ovaries and is upregulated in ovarian endometriosis and pelvic inflammatory disease involving the ovary. Reprod. Sci. *19*, 1197–1204.

Heublein, S., Mayr, D., Vrekoussis, T., Friese, K., Hofmann, S.S., Jeschke, U., and Lenhard, M. (2013). The G-protein coupled estrogen receptor (GPER/GPR30) is a gonadotropin receptor dependent positive prognosticator in ovarian carcinoma patients. PLoS One *8*, e71791.

Hillier, S.G. (1994). Current concepts of the roles of follicle stimulating hormone and luteinizing hormone in folliculogenesis. Hum. Reprod. *9*, 188–191.

Jeppesen, J.V., Kristensen, S.G., Nielsen, M.E., Humaidan, P., Dal Canto, M., Fadini, R., Schmidt, K.T., Ernst, E., and Yding Andersen, C. (2012). LH-receptor gene expression in human granulosa and cumulus cells from antral and preovulatory follicles. J. Clin. Endocrinol. Metab. *97*, E1524–E1531.

Ji, I., Lee, C., Jeoung, M., Koo, Y., Sievert, G.A., and Ji, T.H. (2004). Trans-activation of mutant follicle-stimulating hormone receptors selectively generates only one of two hormone signals. Mol. Endocrinol. *18*, 968–978.

Jiang, X., Fischer, D., Chen, X., McKenna, S.D., Liu, H., Sriraman, V., Yu, H.N., Goutopoulos, A., Arkinstall, S., and He, X. (2014). Evidence for follicle-stimulating hormone receptor as a functional trimer. J. Biol. Chem. *289*, 14273–14282.

Jonas, K.C., Fanelli, F., Huhtaniemi, I.T., and Hanyaloglu, A.C. (2015). Single molecule analysis of functionally asymmetric G protein-coupled receptor (GPCR) oligomers reveals diverse spatial and structural assemblies. J. Biol. Chem. *290*, 3875–3892.

Jonas, K.C., Chen, S., Virta, M., Mora, J., Franks, S., Huhtaniemi, I., and Hanyaloglu, A.C. (2018). Temporal reprogramming of calcium signalling via crosstalk of gonadotrophin receptors that associate as functionally asymmetric heteromers. Sci. Rep. *8*, 2239.

Kamal, F.A., Mickelsen, D.M., Wegman, K.M., Travers, J.G., Moalem, J., Hammes, S.R., Smrcka, A.V., and Blaxall, B.C. (2014). Simultaneous adrenal and cardiac g-protein-coupled receptor-gβγ inhibition halts heart failure progression. J. Am. Coll. Cardiol. *63*, 2549–2557.

Li, Y., Ganta, S., Cheng, C., Craig, R., Ganta, R.R., and Freeman, L.C. (2007). FSH stimulates ovarian cancer cell growth by action on growth factor variant receptor. Mol. Cell. Endocrinol. *267*, 26–37.

Lizneva, D., Rahimova, A., Kim, S.-M., Atabiekov, I., Javaid, S., Alamoush, B., Taneja, C., Khan, A., Sun, L., Azziz, R., et al. (2019). FSH beyond fertility. Front. Endocrinol. (Lausanne). *10*, 136.

Maggiolini, M., Vivacqua, A., Fasanella, G., Recchia, A.G., Sisci, D., Pezzi, V., Montanaro, D., Musti, A.M., Picard, D., and Andò, S. (2004). The G protein-coupled receptor GPR30 mediates c-fos up-regulation by 17beta-estradiol and phytoestrogens in breast cancer cells. J. Biol. Chem. *279*, 27008–27016.

Maillet, G., Bréard, E., Benhaïm, A., Leymarie, P., and Féral, C. (2002). Hormonal regulation of apoptosis in rabbit granulosa cells in vitro: evaluation by flow cytometric detection of plasma membrane phosphatidylserine externalization. Reproduction *123*, 243–251.

Marjon, N.A., Hu, C., Hathaway, H.J., and Prossnitz, E.R. (2014). G protein-coupled estrogen receptor regulates mammary tumorigenesis and metastasis. Mol. Cancer Res. *12*, 1644–1654.

Matoba, A., Matsuyama, N., Shibata, S., Masaki, E., Emala, C.W., and Mizuta, K. (2018). The free fatty acid receptor 1 promotes airway smooth muscle cell proliferation through MEK/ERK and PI3K/Akt signaling pathways. Am. J. Physiol. Lung Cell. Mol. Physiol. *314*, L333–L348.

Moreno, E., Andradas, C., Medrano, M., Caffarel, M.M., Pérez-Gómez, E., Blasco-Benito, S., Gómez-Cañas, M., Pazos, M.R., Irving, A.J., Lluís,

C., et al. (2014). Targeting CB2-GPR55 receptor heteromers modulates cancer cell signaling. J. Biol. Chem. *289*, 21960–21972.

Nechamen, C.A., Thomas, R.M., and Dias, J.A. (2007). APPL1, APPL2, Akt2 and FOXO1a interact with FSHR in a potential signaling complex. Mol. Cell. Endocrinol. *260–262*, 93–99.

Ouelaa-Benslama, R., De Wever, O., Hendrix, A., Sabbah, M., Lambein, K., Land, D., Prévost, G., Bracke, M., Hung, M.-C., Larsen, A.K., et al. (2012). Identification of a GαGβγ, AKT and PKCα signalome associated with invasive growth in two genetic models of human breast cancer cell epithelial-to-mesenchymal transition. Int. J. Oncol. *41*, 189–200.

Pavlik, R., Wypior, G., Hecht, S., Papadopoulos, P., Kupka, M., Thaler, C., Wiest, I., Pestka, A., Friese, K., and Jeschke, U. (2011). Induction of G protein-coupled estrogen receptor (GPER) and nuclear steroid hormone receptors by gonadotropins in human granulosa cells. Histochem. Cell Biol. *136*, 289–299.

Perales-Puchalt, A., Wojtak, K., Duperret, E.K., Yang, X., Slager, A.M., Yan, J., Muthumani, K., Montaner, L.J., and Weiner, D.B. (2019). Engineered DNA vaccination against follicle-stimulating hormone receptor delays ovarian cancer progression in animal models. Mol. Ther. *27*, 314–325.

Polyzos, N.P., and Sunkara, S.K. (2015). Sub-optimal responders following controlled ovarian stimulation: an overlooked group? Hum. Reprod. *30*, 2005–2008.

Ponikwicka-Tyszko, D., Chrusciel, M., Stelmaszewska, J., Bernaczyk, P., Sztachelska, M., Sidorkiewicz, I., Doroszko, M., Tomaszewski, J., Tapanainen, J.S., Huhtaniemi, I., et al. (2016). Functional expression of FSH receptor in endometriotic lesions. J. Clin. Endocrinol. Metab. *101*, 2905–2914.

Prossnitz, E.R., and Hathaway, H.J. (2015). What have we learned about GPER function in physiology and disease from knockout mice? J. Steroid Biochem. Mol. Biol. *153*, 114–126.

Prossnitz, E.R., and Maggiolini, M. (2009). Mechanisms of estrogen signaling and gene expression via GPR30. Mol. Cell. Endocrinol. *308*, 32–38.

Revankar, C.M., Vines, C.M., Cimino, D.F., and Prossnitz, E.R. (2004). Arrestins block G protein-coupled receptor-mediated apoptosis. J. Biol. Chem. *279*, 24578–24584.

Revankar, C.M., Cimino, D.F., Sklar, L.A., Arterburn, J.B., and Prossnitz, E.R. (2005). A transmembrane intracellular estrogen receptor mediates rapid cell signaling. Science *307*, 1625–1630.

Rivero-Müller, A., Chou, Y.-Y., Ji, I., Lajic, S., Hanyaloglu, A.C., Jonas, K., Rahman, N., Ji, T.H., and Huhtaniemi, I. (2010). Rescue of defective G protein-coupled receptor function in vivo by intermolecular cooperation. Proc. Natl. Acad. Sci. U. S. A. *107*, 2319–2324.

Rossi, V., Lispi, M., Longobardi, S., Mattei, M., Di Rella, F., Salustri, A., De Felici, M., and Klinger, F.G. (2017). LH prevents cisplatin-induced apoptosis in oocytes and preserves female fertility in mouse. Cell Death Differ *24*, 72–82.

Rozenfeld, R., Gupta, A., Gagnidze, K., Lim, M.P., Gomes, I., Lee-Ramos, D., Nieto, N., and Devi, L.A. (2011). AT1R-CB$_1$R heteromerization reveals a new mechanism for the pathogenic properties of angiotensin II. EMBO J. *30*, 2350–2363.

Santi, D., Potì, F., Simoni, M., and Casarini, L. (2018). Pharmacogenetics of G-protein-coupled receptors variants: FSH receptor and infertility treatment. Best Pract. Res. Clin. Endocrinol. Metab. *32*, 189–200.

Sasson, R., Dantes, A., Tajima, K., and Amsterdam, A. (2003). Novel genes modulated by FSH in normal and immortalized FSH-responsive cells: new insights into the mechanism of FSH action. FASEB J. *17*, 1256–1266.

Sayers, N., and Hanyaloglu, A.C. (2018). Intracellular follicle-stimulating hormone receptor trafficking and signaling. Front. Endocrinol. (Lausanne). *9*, 653.

Sharma, G., and Prossnitz, E.R. (2016). GPER/GPR30 knockout mice: effects of GPER on metabolism. Methods Mol. Biol. *1366*, 489–502.

Sirotkin, A.V., Benco, A., Tandlmajerova, A., Vasícek, D., Kotwica, J., Darlak, K., and Valenzuela, F. (2008). Transcription factor p53 can regulate proliferation, apoptosis and secretory activity of luteinizing porcine ovarian granulosa cell cultured with and without ghrelin and FSH. Reproduction *136*, 611–618.

Sirotkin, A.V., Ben O, A., Tandlmajerová, A., Lauková, M., Vaší Ek, D., Laurin Ik, J., Kornhauser, J., Alwasel, S., and Harrath, A.H. (2018). cAMP response element-binding protein 1 controls porcine ovarian cell proliferation, apoptosis, and FSH and insulin-like growth factor 1 response. Reprod. Fertil. Dev. *30*, 1145–1153.

Surve, C.R., Lehmann, D., and Smrcka, A.V. (2014). A chemical biology approach demonstrates G protein βγ subunits are sufficient to mediate directional neutrophil chemotaxis. J. Biol. Chem. *289*, 17791–17801.

Tajima, K., Hosokawa, K., Yoshida, Y., Dantes, A., Sasson, R., Kotsuji, F., and Amsterdam, A. (2002). Establishment of FSH-responsive cell lines by transfection of pre-ovulatory human granulosa cells with mutated p53 (p53val135) and Ha-ras genes. Mol. Hum. Reprod. *8*, 48–57.

Thomas, P., Pang, Y., Filardo, E.J., and Dong, J. (2005). Identity of an estrogen membrane receptor coupled to a G protein in human breast cancer cells. Endocrinology *146*, 624–632.

Tranchant, T., Durand, G., Gauthier, C., Crépieux, P., Ulloa-Aguirre, A., Royère, D., and Reiter, E. (2011). Preferential β-arrestin signalling at low receptor density revealed by functional characterization of the human FSH receptor A189 V mutation. Mol. Cell. Endocrinol. *331*, 109–118.

Tubio, M.R., Fernandez, N., Fitzsimons, C.P., Copsel, S., Santiago, S., Shayo, C., Davio, C., and Monczor, F. (2010). Expression of a G Protein-coupled Receptor (GPCR) leads to attenuation of signaling by other GPCRs. J. Biol. Chem. *285*, 14990–14998.

Ulloa-Aguirre, A., Reiter, E., and Crépieux, P. (2018). FSH receptor signaling: complexity of interactions and signal diversity. Endocrinology *159*, 3020–3035.

Wallach, E.E., Shoham, Z., and Schachter, M. (1996). Estrogen biosynthesis—regulation, action, remote effects, and value of monitoring in ovarian stimulation cycles. Fertil. Steril. *65*, 687–701.

Webb, R., Buratini, J., Hernandez-Medrano, J.H., Gutierrez, C.G., Campbell, B.K., Webb, R., Buratini, J., Hernandez-Medrano, J.H., Gutierrez, C.G., and Campbell, B.K. (2016). Follicle development and selection: past, present and future. Anim. Reprod. *13*, 234–249.

Yoshida, Y., Hosokawa, K., Dantes, A., Tajima, K., Kotsuji, F., and Amsterdam, A. (2000). Theophylline and cisplatin synergize in down regulation of BCL-2 induction of apoptosis in human granulosa cells transformed by a mutated p53 (p53 val135) and Ha-ras oncogene. Int. J. Oncol. *17*, 227–235.

iScience, Volume *23*

Supplemental Information

Membrane Estrogen Receptor (GPER) and Follicle-Stimulating Hormone Receptor (FSHR) Heteromeric Complexes Promote Human Ovarian Follicle Survival

Livio Casarini, Clara Lazzaretti, Elia Paradiso, Silvia Limoncella, Laura Riccetti, Samantha Sperduti, Beatrice Melli, Serena Marcozzi, Claudia Anzivino, Niamh S. Sayers, Jakub Czapinski, Giulia Brigante, Francesco Potì, Antonio La Marca, Francesco De Pascali, Eric Reiter, Angela Falbo, Jessica Daolio, Maria Teresa Villani, Monica Lispi, Giovanna Orlando, Francesca G. Klinger, Francesca Fanelli, Adolfo Rivero-Müller, Aylin C. Hanyaloglu, and Manuela Simoni

List of supplementary materials

Supplementary Images

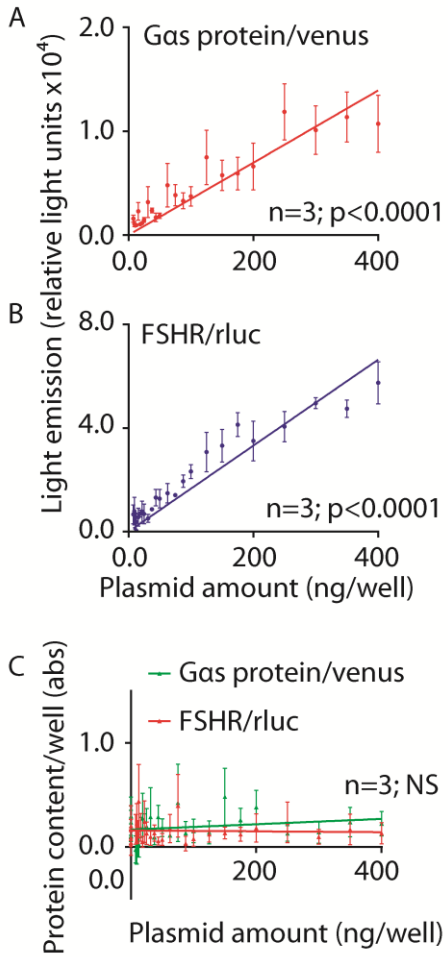

Figure S1. Control of cell transfection efficiency using FSHR and Gαs BRET biosensors. (**A**, **B**) Linear correlation between amount of Gαs protein/venus- or FSHR/rluc-encoding plasmid administered per well, and amount of protein by transiently transfected HEK293 cells. Light emitted by the biosensors was measured by BRET and coelenterazine H was added as a substrate in samples expressing the FSHR/rluc-encoding plasmid 5 min before signal acquisition. Data (means ± SEM; n=3) were interpolated by linear regression forced to pass through x=0.0 and y=0.0. (**C**) Bradford's assay of HEK293 cells transfected with increasing concentrations of Gαs protein/venus- or FSHR/rluc-encoding plasmid (BRET loading control). Protein content was determined by 595 nm absorbance (means ± SEM; n=3) and data interpolated by linear regression. Related to Figure 1A.

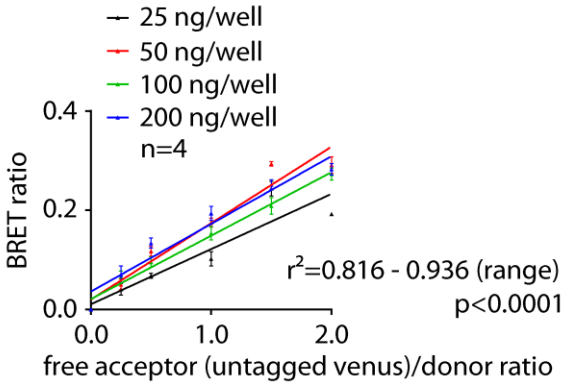

Figure S2. Negative control of FSHR/rluc and venus BRET signal specificity. HEK293 cells were transfected with the indicated concentrations of FSHR/rluc- and with increasing amount of untagged venus-encoding plasmid, then BRET signals were acquired by a plate reader and plotted as means ± SEM against acceptor/donor ratio (n=4). Data were interpolated by linear regression demonstrating the unspecific interaction between FSHR/rluc and untagged venus molecules. Related to Figure 1B-E.

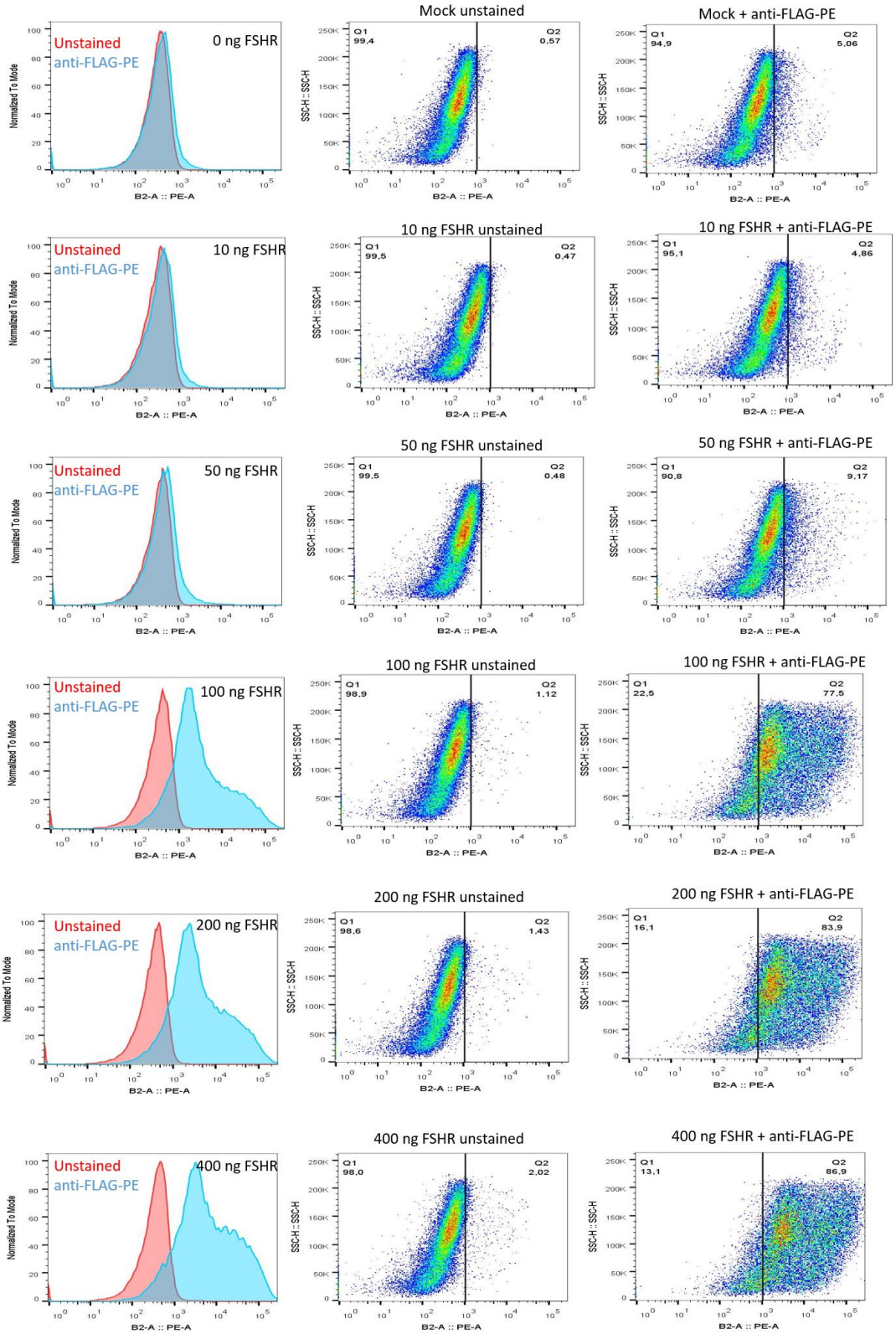
Unstained
anti-FLAG-PE
0 ng FSHR
Mock unstained
Mock + anti-FLAG-PE
10 ng FSHR
10 ng FSHR unstained
10 ng FSHR + anti-FLAG-PE
50 ng FSHR
50 ng FSHR unstained
50 ng FSHR + anti-FLAG-PE
100 ng FSHR
100 ng FSHR unstained
100 ng FSHR + anti-FLAG-PE
200 ng FSHR
200 ng FSHR unstained
200 ng FSHR + anti-FLAG-PE
400 ng FSHR
400 ng FSHR unstained
400 ng FSHR + anti-FLAG-PE
Normalized To Mode
SSC-H :: SSC-H
B2-A :: PE-A
Q1 99,4
Q2 0,57
Q1 94,9
Q2 5,06
Q1 99,5
Q2 0,47
Q1 95,1
Q2 4,86
Q1 99,5
Q2 0,48
Q1 90,8
Q2 9,17
Q1 98,9
Q2 1,12
Q1 22,5
Q2 77,5
Q1 98,6
Q2 1,43
Q1 16,1
Q2 83,9
Q1 98,0
Q2 2,02
Q1 13,1
Q2 86,9

Figure S3. Flow cytometry analysis of plasma membrane FSHR expression levels at different concentrations. 5 x 10^5 HEK293 cells were transfected either with mock vector or increasing concentrations of FLAG-FSHR-encoding plasmid (10-400 ng/well). Then, cells were stained with anti-FLAG-PE antibody for detection of FSHR and analyzed by flow cytometry. Red peaks in histograms refer to unstained cells while light blue peaks refer to cells incubated with anti-FLAG-PE. Total number of cells in each peak was normalized to 100 % (normalized to mode). Dot-plots show side-scatter versus PE-intensity. Q1 represents the percentage of unstained cells and Q2 the percentage of stained cells for each dot-plot. Related to Figure 1B-E.

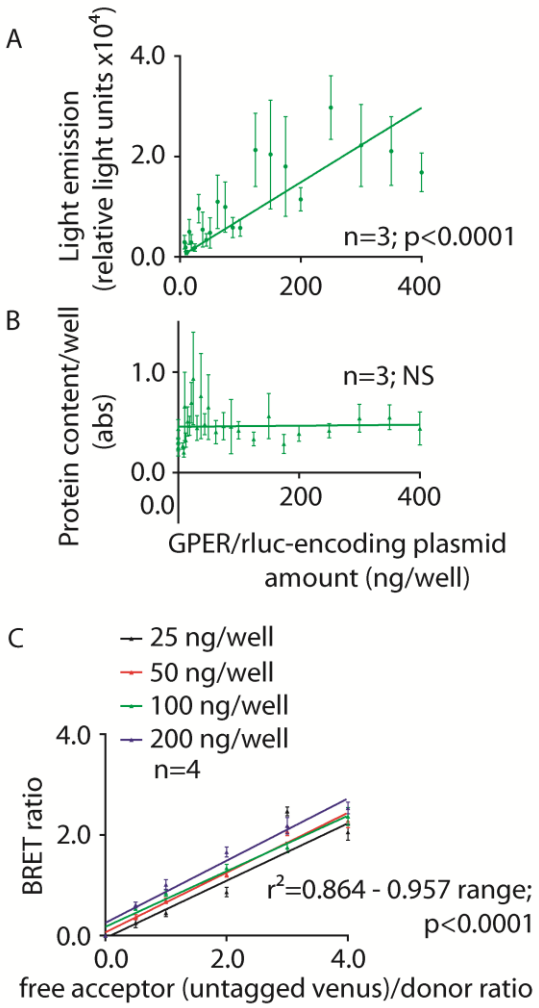

Figure S4. Control of cell transfection efficiency and signal specificity using the GPER BRET biosensors. (**A**) Linear correlation between amount of GPER/rluc-encoding plasmid per well and protein encoded, in transfected HEK293 cells. Light emitted by the biosensors was measured by BRET 5 min after addition of coelenterazine H. Data were interpolated by linear regression forced to pass through x=0.0 and y=0.0 (means ± SEM; n=3). (**B**) BRET loading control determined by Bradford's assay. HEK293 cells were transfected with increasing concentrations of GPER/rluc-encoding plasmid and the protein content was detected (absorbance at 595 nm), plotted as means ± SEM against the amount of plasmid per well and interpolated by linear regression (n=3). (**C**) Negative control of GPER/rluc and venus BRET signal specificity. HEK293 cells were transfected with the indicated concentrations of GPER/rluc- and with increasing amount of untagged venus-encoding plasmid, then BRET signals were acquired and plotted against the

acceptor/donor ratio (means ± SEM; n=4). Data interpolation by linear regression demonstrates the unspecific interaction between GPER/rluc and untagged venus molecules. Related to Figure 2F.

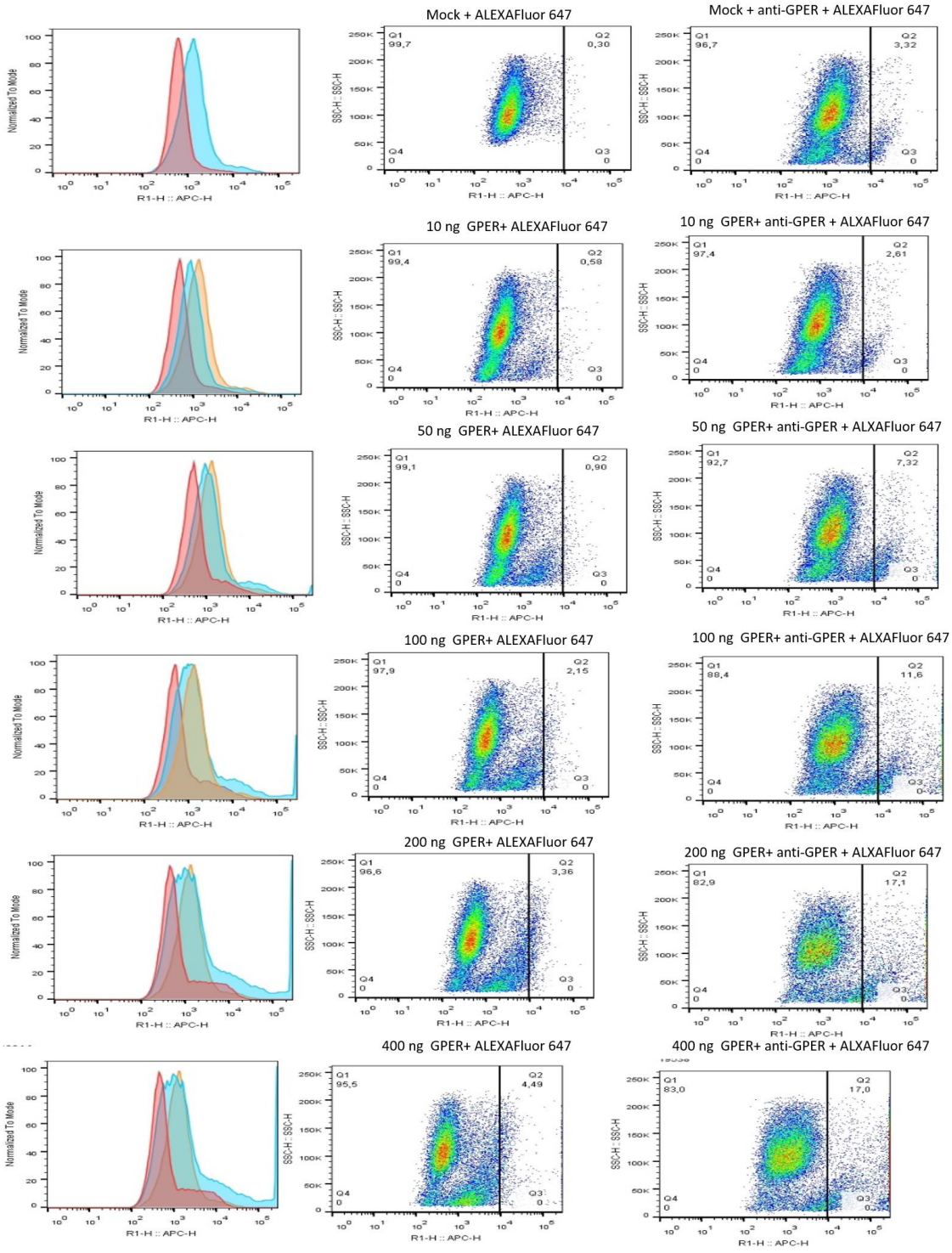

Figure S5. Flow cytometry analysis of plasma membrane GPER expression levels at different concentrations. 5 x 10^5 HEK293 cells were transfected either with mock vector or increasing concentrations of GPER-encoding plasmid (10-400 ng). Then, cells were

incubated with anti-GPER primary antibody followed by incubation with ALEXA Fluor 647 secondary antibody and analyzed by flow cytometry. Red peaks in histograms refer to cells incubated with secondary antibody only, light blue peaks refer to cells incubated with primary and secondary antibody while orange peaks refer to mock-transfected cells incubated with primary and secondary antibodies. Total number of cells in each peak was normalized to 100 % (normalized to mode). Dot-plots show side-scatter versus ALEXA Fluor 647 (APC-H) intensity. Q1 represents the percentage of cells negative to ALEXA FLUOR 647 staining and Q2 the percentage of cells positive to ALEXA FLUOR 647 staining in each dot-plot. Related to Figure 2F.

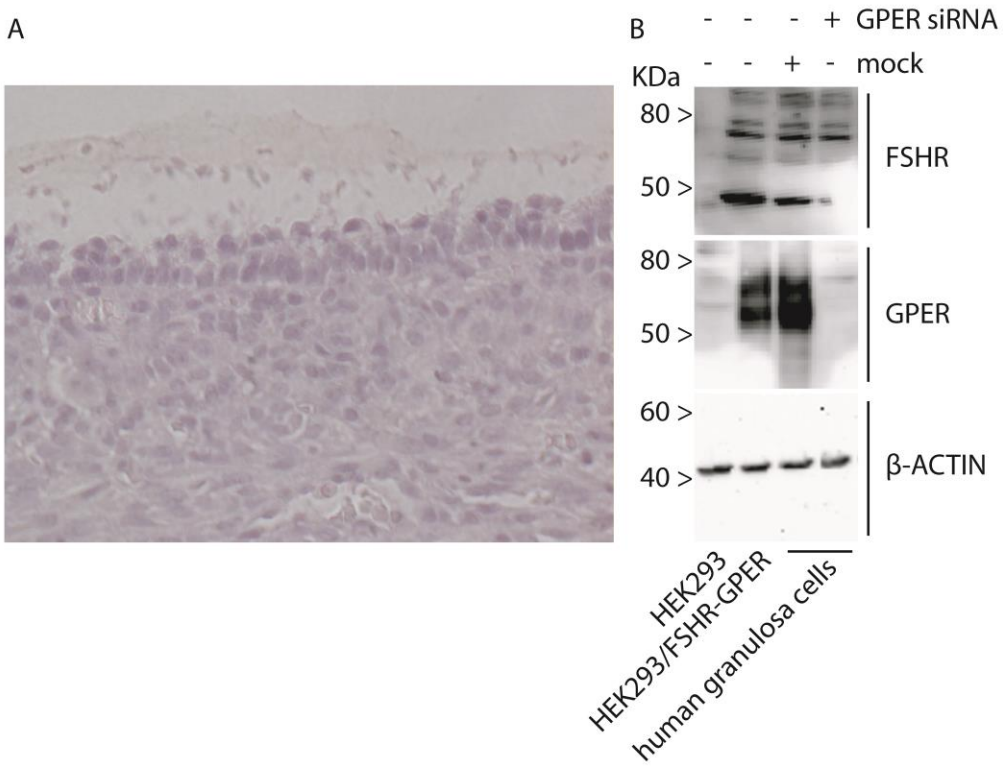

Figure S6. Antibody validations (**A**) Control section of IHC for FSHR and GPER. The same area was analyzed in serial sections, respectively incubated with anti-FSHR or anti-GPER antibodies or in absence of primary antibody (control). No staining was observed in this area indicating the specific signal of FSHR and GPER. (**B**) Uncropped Western blotting pictures using anti-FSHR, -GPER and -β-ACTIN antibodies (Fig. 1C). Membrane incubation with anti-FSHR antibody results in a number of known bands, as previously described (Casarini et al., 2016). The anti-GPER antibody may produce 52-58 KDa bands, as described by studies (Cheng et al., 2014) and providers (see: https://www.genetex.com/Product/Detail/GPR30-antibody-C2C3-C-term/GTX107748, last accession on April, 25th 2020). Related to Figure 6A, B, D.

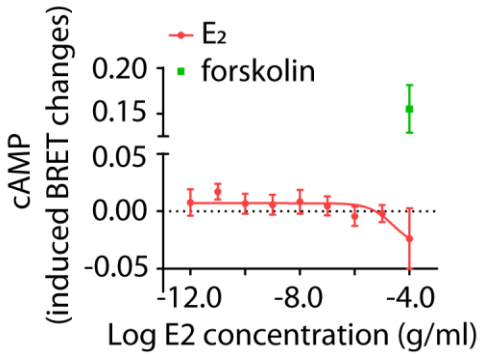

Figure S7. Failure of E_2-induced cAMP increase via GPER. Transfected HEK293 cells expressing GPER and the cAMP biosensor CAMYEL were treated 30 min with increasing E_2 concentrations (1.0 pg/ml-100 µg/ml range), in the presence of the phosphodiesterase inhibitor IBMX, before cAMP measurement by BRET. Results were represented in the x-y graph as means ± SEM (n=5) and interpolated by non-linear regression. No significantly different cAMP levels *versus* the vehicle were found, except for the forskolin-treated cells serving as positive controls (two-way ANOVA with Sidak's correction for multiple tests; $p<0.000$). Related to Figure 3C.

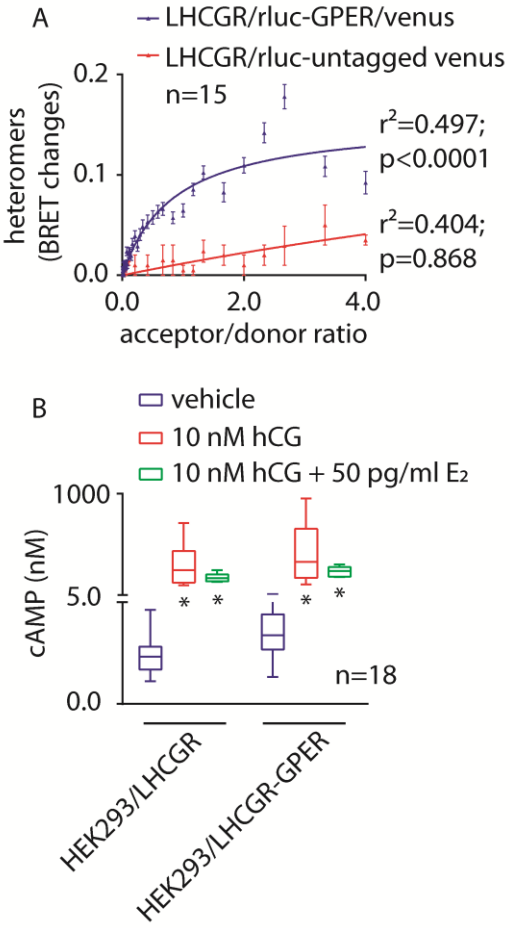

Figure S8. hCG-induced cAMP increase in the presence of LHCGR and GPER heteromers. (**A**) BRET signal demonstrating the formation of LHCGR/rluc- and GPER/venus-tagged heteromers, in transfected HEK293 cells. BRET ratio values resulting from molecular interactions were represented in the x-y graph as means ± SEM (n=5). Specific binding is indicated by data interpolation using non-linear regression, which results in the logarithmic curve, while unspecific binding between LHCGR/rluc and untagged venus molecules is indicated by linear regression. (**B**) 10 nM hCG-induced intracellular cAMP increase, in HEK293 cells expressing either one or both LHCGR and GPER. 50 pg/ml E_2 was added as indicated. cAMP was measured by ELISA and represented by box and whiskers plots (*=significantly different *versus* vehicle-treated HEK293/LHCGR; two-way ANOVA with Sidak's correction for multiple tests; $p<0.0001$; n=18). Related to Figure 3F.

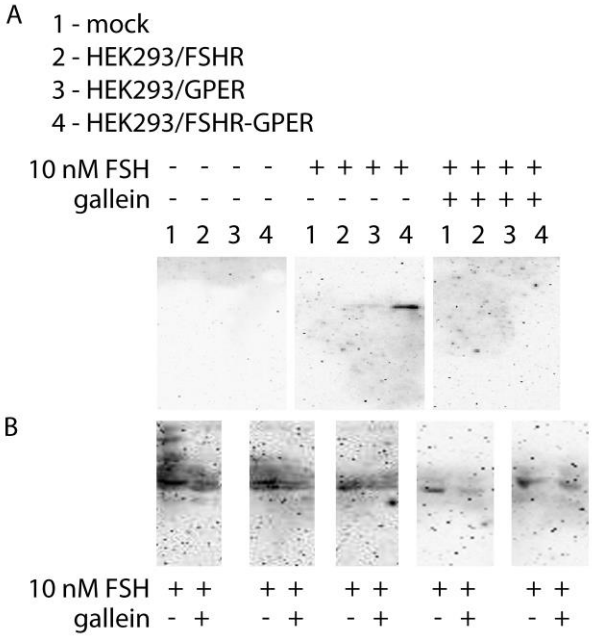

Figure S9. Western blotting analysis of FSH-induced pAKT activation. (**A**) Uncropped Western blotting pAKT membranes of Fig. 4H. (**B**) Experimental replicates of pAKT activation in HEK293/FSHR-GPER cells treated by FSH, in the presence or in the absence of gallein. Signals were acquired by the QuantityOne analysis software (Bio-Rad Laboratories Inc.) and plotted on a box and whiskers graph (Fig. 4I) after background subtraction. Related to Figure 3H.

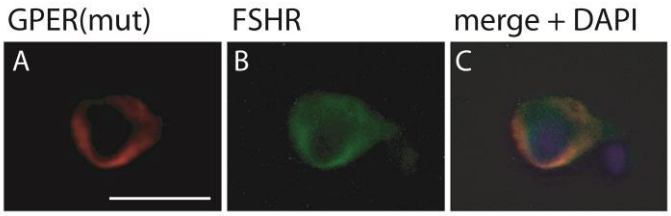

Figure S10. Representative evaluation of GPER(mut) and FSHR co-localization by immunofluorescence, in transfected HEK293 cells. GPER(mut) was detected by the anti-GPER specific primary antibody and TRITC-labelled secondary antibody, while FSHR is identified by the venus tag light emission. Nuclei were blue-stained by DAPI (bar=25 μm). Related to Figure 4G.

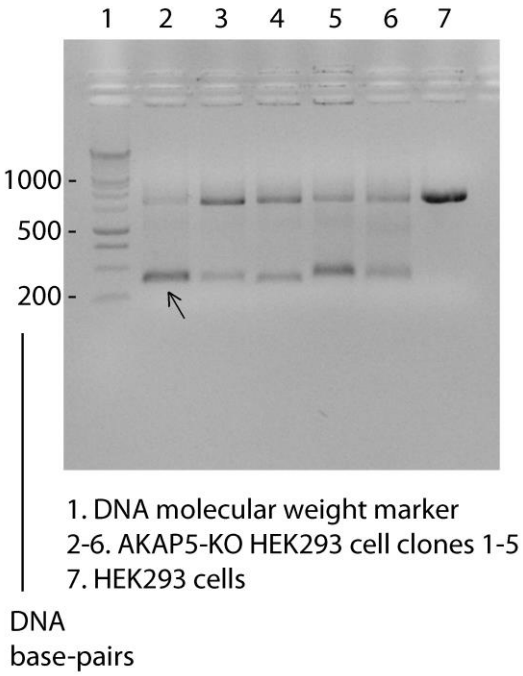

Figure S11. Screening of *AKAP5*-KO HEK293 cells by PCR and 1% agarose-gel electrophoresis. *AKAP5* forward (fwd) and reverse (rev) primers (*GGAGTAAGATGAAAGGTATGAATATGCC* and *CTGCAATCTGTGCTGACTTCC*, respectively; 58°C melting temperature) were designed using the human gene sequence as a template (NC_000014.9). PCR reactions were performed using genomic DNAs extracted from five KO clones (lanes 2-6), while DNA from “native” HEK293 cells was used as a control (lane 7). The predicted sequenced amplified in *AKAP5*-KO cells is of 335 base-pairs, while a band of about 900 base-pairs is predicted to be amplified in the WT *AKAP5*-positive sample. A variable grade of *AKAP5*-WT cell contamination persists among the cultured *AKAP5*-KO HEK293 cells maintained under selective pressure by 1.2 µg/ml puromycin. Arrow indicates the clone used for experiments (Fig. 5). Related to Figure 5A.

Figure S12. *AKAP5* gene and CRISPR/Cas9 targeting. The entire coding region in exon 2 was erased. Sequence of the Cas9 backbone carried in pSpCas9(BB)-2A-Puro (PX459) V2.0 vectors are below and gRNA sequences indicated in bold. Related to Figure 5A.

5’-
AMMTCGMMAWWACGATACAAGCTGTTAGAGAGATAATTGGAATTAATTTGACTGT
AAACACAAAGATATTASTACAAAATACGTGACGTAGAAAGTAATAATTTCTTGGGTA
GTTTGCAGTTTTAAAATTATGTTTTAAAATGGACTATCATATGCTTACCGTAACTTGA
AAGTATTTCGATTTCTTGGCTTTATATATCTTGTGGAAAGGACGAAA**CACCGATCAG**
CAGAAGGTAGTCCTGGTTTTAGAGCTAGAAATAGCAAGTTAAAATAAGGCTAGTCC
GTTATCAACTTGAAAAAGTGGCACCGAGTCGGTGCTTTTTTGTTTTAGAGCTAGAAA
TAGCAAGTTAAAATAAGGCTAGTCCGTTTTTAGCGCGTGCGCCAATTCTGCAGACA
AATGGCTCTAGAGGTACCCGTTACATAACTTACGGTAAATGGCCCGCCTGGCTGA
CCGCCCAACGACCCCCGCCCATTGACGTCAATAGTAACGCCAATAGGGACTTTCC
ATTGACGTCAATGGGTGGAGTATTTACGGTAAACTGCCCACTTGGCAGTACATCAA
GTGTATCATATGCCAAGTACGCCCCCTATTGACGTCAATGACGGTAAATGGCCCGC
CTGGCATTGTGCCCAGTACATGACCTTATGGGACTTTCCTACTTGGCAGTACATCT
ACGTATTAGTCATCGCTATTACCATGGTCGAGGTGAGCCCCACGTTCTGCTTCACT
CTCCCCATCTCCCCCCCCTCCCCACCCCCAATTTTGTATTTATTTATTTTTTAATTAT
TTTGTGCAGCGATGGGGGCGGGGGGGGGGGGGGGGG-3’

5’-
ACMMMCGCMWWAMGATAMAAGGCTGTTAGAGAGATAATTGGAATTAATTTGACT
GTAAACACAAAGATATTAGTACAAAATACGTGACGTAGAAAGTAATAATTTCTTGGG
TAGTTTGCAGTTTTAAAATTATGTTTTAAAATGGACTATCATATGCTTACCGTAACTT
GAAAGTATTTCGATTTCTTGGCTTTATATATCTTGTGGAAAGGACGAAA**CACCGTGA**
CTTACTCTCCAGAGTCAGTTTTAGAGCTAGAAATAGCAAGTTAAAATAAGGCTAGT
CCGTTATCAACTTGAAAAAGTGGCACCGAGTCGGTGCTTTTTTGTTTTAGAGCTAG
AAATAGCAAGTTAAAATAAGGCTAGTCCGTTTTTAGCGCGTGCGCCAATTCTGCAG
ACAAATGGCTCTAGAGGTACCCGTTACATAACTTACGGTAAATGGCCCGCCTGGCT
GACCGCCCAACGACCCCCGCCCATTGACGTCAATAGTAACGCCAATAGGGACTTT

CCATTGACGTCAATGGGTGGAGTATTTACGGTAAACTGCCCACTTGGCAGTACATC
AAGTGTATCATATGCCAAGTACGCCCCCTATTGACGTCAATGACGGTAAATGGCCC
GCCTGGCATTGTGCCCAGTACATGACCTTATGGGACTTTCCTACTTGGCAGTACAT
CTACGTATTAGTCATCGCTATTACCATGGTCGAGGTGAGCCCCACGTTCTGCTTCA
CTCTCCCCATCTCCCCCCCCTCCCCACCCCCAATTTTGTATTTATTTATTTTTTAATT
ATTTTGTGCAGCGATGGGGGCGGGGGGGGGGGGGGGGSC-3’

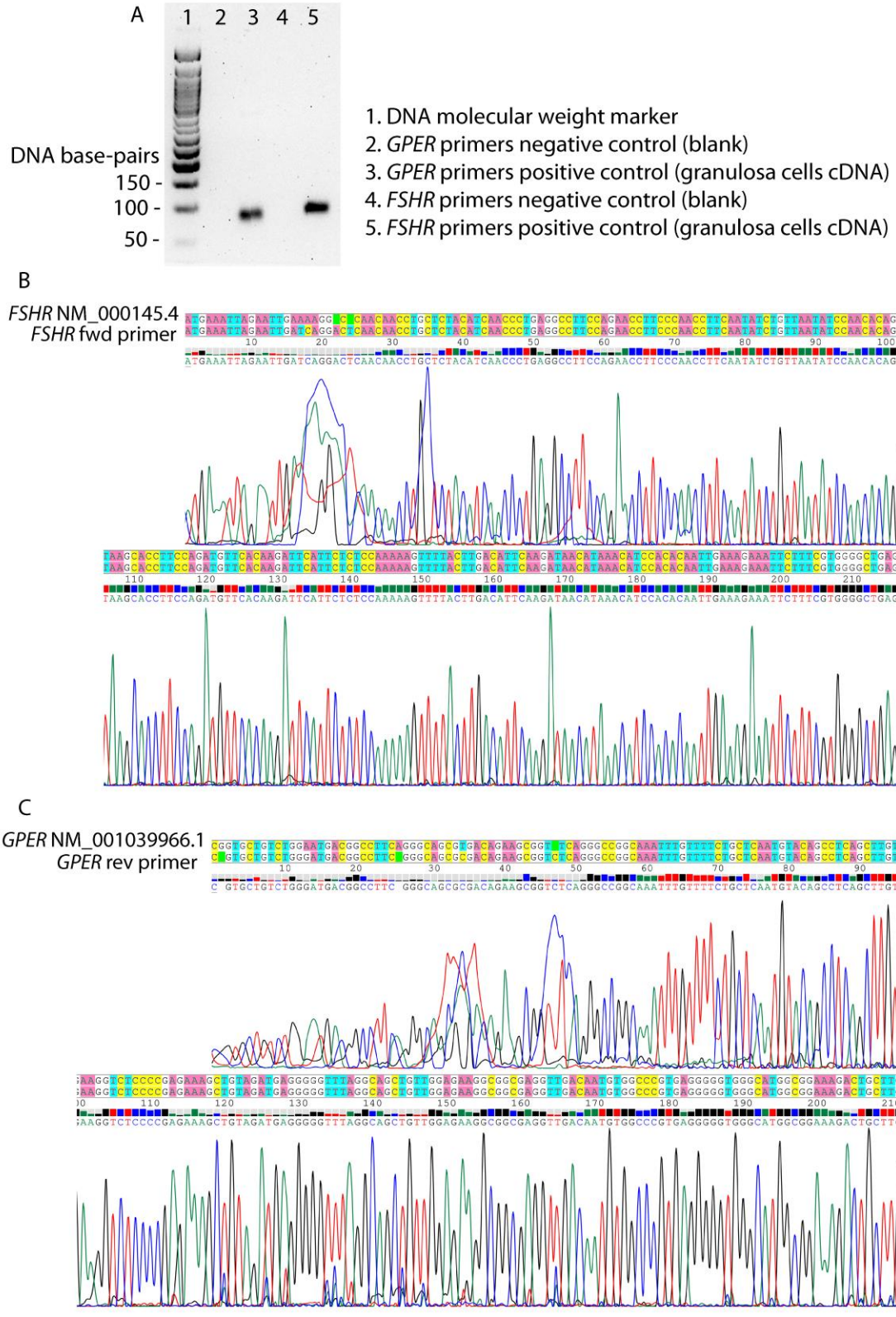
A
1 2 3 4 5
DNA base-pairs
150 -
100 -
50 -
1. DNA molecular weight marker
2. GPER primers negative control (blank)
3. GPER primers positive control (granulosa cells cDNA)
4. FSHR primers negative control (blank)
5. FSHR primers positive control (granulosa cells cDNA)
B
FSHR NM_000145.4
FSHR fwd primer
C
GPER NM_001039966.1
GPER rev primer

Figure S13. Validation of the *FSHR* and *GPER* primer sequences used for real-time PCR analyses. (**A**) Control experiment performed using blank samples and cDNAs from human primary granulosa cells. Analysis by PCR and 1% agarose-gel electrophoresis demonstrates the presence of bands at the predicted molecular weights. (**B**, **C**) Images of partial electropherograms obtained by DNA Sanger's sequencing demonstrating the specificity of the primers used for real-time PCRs displayed in the figure 6 (only one of the two primers per gene is shown). FSHR and GPER BRET plasmids were used as templates. Related to Figure 6D.

Figure S14. Normalizer (*RPS7*) gene expression raw data. Data were obtained from two technical replicates by real-time PCR analysis of normo- and sub-responder women cDNAs. *FSHR* and *GPER* gene expression increase over the *RPS7* level are also indicated. Related to Figure 6D.

Patient ID	**FSHR (fold-increase over *RPS7*)**	**GPER (fold-increase over *RPS7*)**		***RPS7* mean Cq**
		normo-responders	**sub-responders**	
1	0.89	0.87		27.34
3	0.82	0.80		24.51
5	0.89	0.92		28.50
6	0.81	0.79		24.34
7	0.85	0.82		25.32
8	0.84		0.84	25.23
9	0.83		0.85	25.56
10	0.80	0.81		24.99
11	0.81	0.83		24.29
12	0.83	0.82		24.71
13	0.82	0.91		26.92
14	0.81		0.99	31.18
15	0.75		0.88	27.25
16	0.88	0.86		26.89
17	0.85		0.82	25.38
18	0.89	0.86		27.68
19	0.83	0.80		23.77
20	0.72		0.86	23.90
21	0.85	0.87		26.63
22	0.80		0.89	27.18
23	0.78		0.79	23.91
24	0.82	0.81		25.86
25	0.83	0.83		26.32
26	0.87		0.86	26.59
27	0.85	0.84		24.68
28	0.82	0.89		24.37
30	0.86	0.81		26.75
31	0.86		0.84	29.16
32	0.82		0.80	25.83
33	0.84		0.84	28.77
38	0.87	0.87		25.66
40	1.07		0.86	29.79
41	0.76	0.79		25.13
42	0.86	0.91		26.19

45	0.79		0.83	26.13
47	0.92	0.79		26.18
48	0.82	0.75		25.77
52	1.18		0.94	26.40
53	0.98		0.88	25.20
54	0.75	0.76		29.03
55	0.82	0.82		32.44
56	0.71	0.78		28.80
61	0.92	0.82		27.50
63	0.98		0.82	25.86
64	0.70	0.76		28.10
67	0.82		0.82	25.21
70	0.84	0.80		27.21
72	0.82		0.80	28.16
73	0.80	0.80		27.90
74	0.78	0.79		24.57
75	0.88	0.89		26.20
76	0.86	0.87		26.73
77	0.97		0.93	26.88
78	0.94	0.89		27.30
79	0.94	0.90		28.29
82	0.86	0.91		25.68
83	0.79	0.82		28.11
87	0.91	0.93		24.68
88	0.96	0.95		28.59
89	0.89		0.84	28.95
90	1.12	1.12		29.62
91	0.80		0.85	25.04
92	0.73	0.75		26.77
93	0.80	0.77		30.55
94	0.71		0.76	26.00
95	0.83	0.78		26.85
96	0.84		0.78	23.95
97	0.81		0.77	34.32
99	0.86	0.84		31.00
100	0.85		0.81	23.21
101	0.88		0.86	26.09
102	0.87		0.85	24.33
103	0.83		0.80	26.36
104	0.84	0.78		28.42
105	0.91	0.87		23.42
106	1.00	0.99		25.90
107	0.91	0.92		27.19
108	0.83	0.79		29.45
109	0.85	0.77		27.00

110	0.95	0.92		27.26
111	0.86	0.81		30.49
112	0.84	0.83		29.14
113	0.80	0.76		32.76
115	0.78	0.74		30.02
118	0.85	0.77		29.69
119	0.97	0.93		29.17
120	1.03	0.98		25.51
121	NA	NA		25.14
122	1.09	1.01		24.15
123	0.98	0.96		26.37
124	0.93	0.84		25.16
125	0.84		0.77	27.13

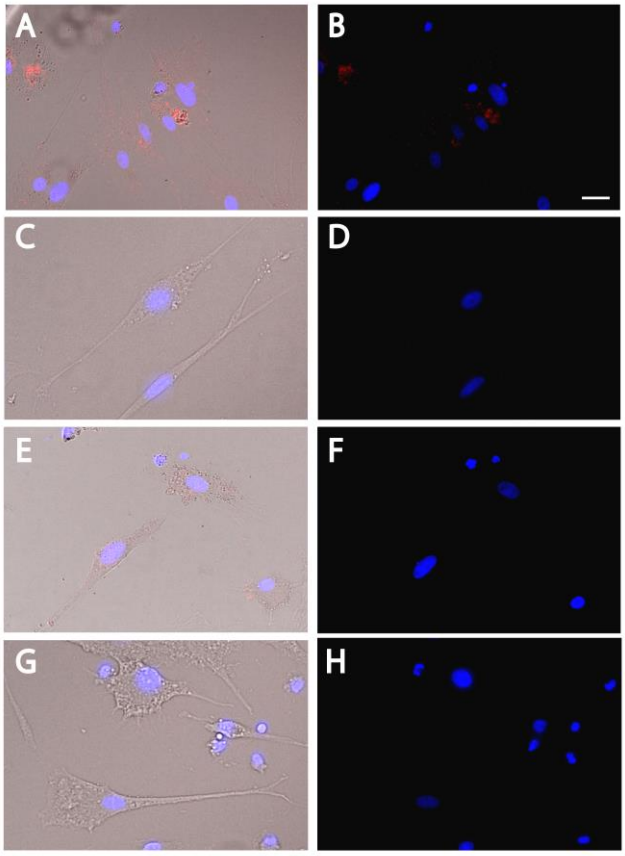

Figure S15. Representative evaluation of FSHR-GPER interaction by proximity ligation assay. Fixed human primary granulosa cells were treated by specific primary antibodies against GPER and FSHR before sample incubation with “PLUS” and “MINUS” probes, and red detection reagents (see Supplementary materials and methods). Nuclei were blue-stained by DAPI and signals captured by a fluorescent microscope (bar=40 μm); images representative of three independent experiments. (**A, B**) Bright field and fluorescence images of positive (red) signals indicating FSHR-GPER interaction. (**C, D**) Negative controls obtained in the absence of the “PLUS” probe. (**E, F**) Negative controls, absence of the “MINUS” probe. (**G, H**) Negative controls prepared without incubation with primary antibodies. Related to Figure 6C, E-J.

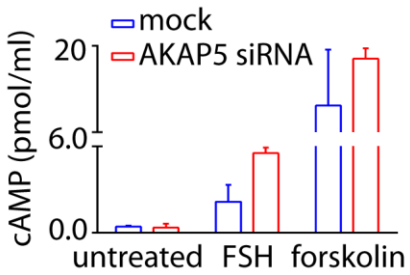

Figure S16. FSH-induced cAMP increase under 48-h AKAP5 knockdown by siRNA. Human primary granulosa cells were treated 30 min with 10 nM FSH, in the presence of IBMX, before cAMP measurement by HTRF. Results are means ± SD of two experiments and forskolin-treated samples served as positive controls. FSH treatment induced 2.6-fold FSH levels in AKAP5-depleted than mock-transfected cells. Related to Figure 6K.

Transparent Methods

Study design.

The objective of this study in vitro was to determine the impact of FSHR-GPER heteromers in modulating FSH impact on cell viability. Experiments were performed in biological triplicate, unless otherwise stated, on the basis of previous experiences using transfected cell lines and primary cells in vitro. Studies with granulosa cells collected from donor poor- and normo-responder women undergoing oocyte retrieval for assisted reproduction techniques were performed with n=30 and 61 samples, which have a power of about 95% to detect a difference of 1.7% between the r2 values of two groups (alpha=0.05). Experiments were blinded to the operator performing cell handling and real-time PCR analyses. Written consent was collected from women under local Ethics Committee permission (Nr. 796 19th June 2014, Reggio Emilia, Italy). Patients matched these criteria: absence of endocrine abnormalities and viral/bacterial infections, age between 25 and 45 years.

Cell lines and reagents.

The HEK293 cell line was available in-house and previously validated for BRET experiments (Lazzaretti et al., 2019; Riccetti et al., 2017a). The culture medium was Dulbecco's Modified Eagles Medium (DMEM) enriched by 10% fetal bovine serum (FBS), 2 mM L-glutammine, 100 U/ml penicillin and 50 µg/ml streptomycin.

Human primary granulosa cells were collected from ovarian follicles of donor women classified as poor- (≤4 oocytes collected after controlled ovarian stimulation) or normo-responders (>4 oocytes), as indicated by a previous consensus paper (Ferraretti et al., 2011) and more recent evidences suggesting that ovarian response may be categorized as poor, suboptimal, normal and high (Polyzos and Sunkara, 2015). Women were clinically treated in a GnRH antagonist protocol, where ovarian stimulation was performed by FSH and oocyte trigger with hCG. Normo- and sub-responder groups differ for the number of oocytes (8.1 ± 3.2 *vs* 2.6 ± 1.2, respectively), serum E_2 levels at the day of oocytes collection (1895.0 ± 866.9 *vs* 1348.0 ± 838.2 pg/ml) and total FSH

dose for achieving the oocyte maturation (2895.0 ± 4378.0 *vs* 3642.0 ± 3010.0 IU; Mann-Whitney's U-test, $p<0.05$), while the duration of the stimulation cycle was similar between the two groups (12.6 ± 3.2 *vs* 13.7 ± 3.5 days; Mann-Whitney's U-test, $p\geq0.05$). Granulosa cells were handled as previously described (Riccetti et al., 2019) and cultured in McCoy's 5A medium, 10% FBS, 2 mM L-glutamine, 100 IU/ml penicillin, 100µg/ml streptomycin and 250 ng/ml Fungizone. All culture reagents were from Sigma-Aldrich (Sigma-Aldrich Corporation, St. Louis, MO, USA).

Recombinant FSH was provided by Merck KGaA (Gonal-f; Merck KGaA, Darmstadt, Germany) and used at the concentration of 10 nM as previously described (Lazzaretti et al., 2019), while E_2 (cat. E8875; 50 pg/ml) (Casarini et al., 2017), 8-br-cAMP (B7880; $1x10^{-15}$-10^{0} nM range) (Lazzaretti et al., 2019), forskolin (F6886; 50 µM) (Casarini et al., 2016), gallein (cat. 371708; 10 µM) (Sanz et al., 2017), fulvestrant (I4409; 2 µg/ml) (Wakeling et al., 1991) and triton-X (T8787; 5%) were purchased by Sigma-Aldrich. Three human GPER siRNA probes (284631; 3x10 µM/probe) were purchased by ThermoFisher Scientific (Waltham, MA, USA) and delivered into cells using the TransIT TKO transfection reagent (Mirus Bio Corporation, Madison, WI, USA). The AKAP5-encoding gene was silenced by using the TriFECTa® RNAi kit (#hs.Ri.AKAP5.13; Integrated DNA Technologies, Coralville, IA, USA). The control siRNA was the #4390843 Silencer™ Negative Control No. 1 siRNA (Thermo Fisher Scientific).

FSHR-, LHCGR-, Ca^{2+} aequorin- and cAMP CAMYEL-encoding BRET biosensor and cFMS plasmids were available in-house and previously validated (Lazzaretti et al., 2019; Riccetti et al., 2017a, 2019; Sposini et al., 2015). GPER- and GPER(mut)-encoding BRET biosensor plasmids were developed by *de novo* synthesis and checked by the producer (Gene Universal Inc., Newark, DE, USA), basing on the FLAG/GPER-encoding plasmid (Albanito et al., 2008) provided by professor Marcello Maggiolini (University of Calabria, Cosenza, Italy). Gα protein-encoding BRET biosensor plasmids (Wan et al., 2018) were kindly provided by professor Nevin A. Lambert (Augusta University, Augusta, GA, USA). Cell transfections using plasmids were performed using Metafectene PRO (Biontex Laboratories GmbH, Munich, Germany).

BRET and HTRF measurements, and ELISA.

Intracellular Ca^{2+} and cAMP levels were evaluated following a validated procedure (Brigante et al., 2019; Casarini et al., 2019; Lazzaretti et al., 2019; Riccetti et al., 2017b, 2017a, 2019), in transiently transfected HEK293 cells. G protein coupling experiments were adapted to optimize BRET signals with GPER- and FSHR-encoding plasmids (100 ng plasmid/well as reference amount), starting from the published validation protocol (Wan et al., 2018). BRET signals were induced using 10 µl/well of 5µM Coelenterazine h (Interchim, Montluçon, France) diluted in 40 µl/well PBS and 1 mM Hepes, in the presence or in the absence of hormones/vehicle. Light emissions were detected at 475±30 and 530±30 nm wavelengths by the CLARIOstar plate reader equipped with a monochromator (BMG Labtech, Ortenberg, Germany). Assessment of protein content was used as loading controls for BRET experiment, while linearity between amount of plasmid administered per well and receptor expressed was confirmed detecting signals of the biosensor-tag.

In granulosa cells and in the GPER(mut)-expressing cell line, cAMP production was measured using an ELISA kit (ab65355; Abcam, Cambridge, UK) following the manufacturer's instructions and signals acquired by a Victor3 plate reader (Perkin Elmer Inc., Waltham, MA, USA). Alternatively, cAMP was measured in granulosa cells by homogeneous time-resolved fluorescence (HTRF) where indicated. The assay was performed using the cAMP dynamic 2 assay kit and following the provider's instructions (CisBio Bioassays, Bagnol sur Cèze, France). Cells were treated with ligands three h in the presence of 50 µM of the phosphodiesterase inhibitor 3-isobutyl-1-methylxanthine (IBMX; Sigma-Aldrich) before to be lysed and transferred into white 384-well microplates. 10 µl/well of the supplied conjugate-lysis buffer, containing d2-labeled cAMP and Europium cryptate-labeled anti-cAMP antibody, was added. Plates were incubated for 1 h in the dark at room temperature and signals measured at 620 and 665 nm, 50 ms after excitation at 320 nm using the CLARIOstar plate reader (BGM Labtec).

Viability assay.

The 3-(4,5-dimethylthiazol-2-yl)-2,5-diphenyltetrazolium bromide (MTT) assay was performed according the manufacturer's instruction and previous optimizations (Casarini et al., 2016, 2017). The assay solution was prepared starting from the powder commercially available (M5655; Sigma-Aldrich) and left into cell well-plates 4 h before to be lysed with isopropanol and determine absorbance value by a plate reader.

PD-PALM imaging and localization analysis.

PD-PALM imaging was carried out as previously described (Jonas et al., 2015). Briefly, anti-FLAG and anti-HA antibodies were labelled with CAGE 500 and 552 photoswitchable dyes, respectively, following manufacturer's protocol (Abberior GmbH, Göttingen, Germany). Degree of labelling was determined to be 1.0 ± 0.2 dye molecules per antibody and 1.3 ± 0.1 dye molecules per antibody for FLAG-CAGE 500 and HA-CAGE 552 respectively. HEK293 cells were transfected with 0.5 µg FLAG-tagged GPER or GPER(mut), and 1 µg HA-tagged FSHR per well of a 6-well plate. Transfected cells were seeded onto 1.5 glass bottom dishes (MatTek Corporation, Ashland, MA, USA). Cells were incubated with CAGE-conjugated antibodies at 37 °C for 30 min. Cells were washed with PBS and fixed in 4% paraformaldehyde with 0.2% glutaraldehyde for 30 min. Cells were washed with DPBS and maintained in DPBS in the dark until imaging. Simultaneous dual-color images were acquired using an Elyra PS1 (Carl Zeiss AG, Oberkochen, Germany). Images were obtained at 100x oil emersion, 1.45 NA objective. Photo-conversion of CAGE 500 and 552 dyes was achieved with 405 nm light source and was simultaneously imaged and photo-bleached by 491 and 561 nm lasers, respectively. Acquisition of images is as previously described (Jonas et al., 2015).

Analysis was carried out on cropped non-overlapping 2 × 2 µm regions, within cell-cell boundaries, from 491- and 561-nm channels and analyzed for localized receptors by QuickPALM Fiji plugin to generate x-y coordinates of localized receptors in each channel. The number of associated protomers derived from the *x-y* coordinates were quantified using a custom Java application (PD-Interpreter) (Jonas et al., 2015). The percentage and protomer composition of FSHR, GPER and GPER(mut) homomers and heteromers was carried out using a second order Getis Franklin neighbourhood analysis with a search radius of 50 nm. This radius has been previously employed for

gonadotrophin hormone receptors based on localization precision, the large extracellular domain of FSHR and the maximum distance that labelling of the antibody would concur, ~15-20 nm (Roberts et al., 1995). Outputted data was represented as a co-localization plot with heat maps generated to represent the different numbers of associated protomers observed.

Protein analysis.

Protein content of samples was determined by the colorimetric Bradford assay using a commercial reagent and following the manufacturer's instructions (#5000201; Bio-Rad Laboratories Inc., Hercules, CA, USA), then 595-nm signals were acquired by a plate reader. Target proteins were analyzed by 12% SDS-PAGE and Western blotting using a validated protocol (Bates et al., 2006; Casarini et al., 2012, 2016, 2017) after extraction in ice-cold RIPA buffer along with PhosStop phosphatase inhibitor and a protease inhibitor cocktail (Roche, Basel, Switzerland). Human pAKT, -pCREB and total ERK (#9271, #9198, #4695, respectively; Cell Signaling Technology Inc., Danvers, MA, USA), active/pro caspase 3 (#MA1-91637; Thermo Fisher Scientific, MA, USA), FSHR (#PA5-28764; ThermoFisher Scientific, Waltham) and GPER (#AF5534; Bio-Techne Corporation, Minneapolis, MN, USA) were evaluated using specific antibodies and secondary anti-rabbit (#NA9340V; GE HealthCare) or -goat HRP-conjugated antibodies (#ab6885; Abcam), as appropriate. A mouse HRP-conjugated anti-human β-ACTIN antibody (#A3854; Sigma-Aldrich) was also used. Signals were developed with ECL (GE HealthCare), detected and semi-quantified by VersaDoc system using the QuantityOne analysis software (Bio-Rad Laboratories Inc.).

Steroid hormone measurements.

Serum FSH levels were calculated as the cumulative dose injected in patients throughout the ovarian stimulation period. Total progesterone and estradiol was measured in sera and in the cell media (4×10^4 cells/well), as indicated, by an immunoassay analyzer (ARCHITECT second Generation system; Abbot Diagnostics, Chicago, IL, USA) after freezing-thawing samples (Riccetti et al., 2019) and data normalized over cell amount.

Structural modeling.

No crystallographic structures are available so far for GPER. Structural models of the two receptors (human species) deprived of the N-terminal and C-terminal regions were achieved by comparative modeling (by the Modeler software (Sali and Blundell, 1993)) by using the crystal structure of an inactive state of the μ-opioid receptor (PDB: 4dkl) as a template, according to a protocol already described (Fanelli and De Benedetti, 2011). As for the FSHR, to model the insertions, the following portions: 488-490 (in E1), 580-583 (in E2), 617-621 and 628-631 (both in I3), and 669-671 (in E3) were deleted in the template crystal structure, followed by addition of external α-helical restraints to the following amino acid stretches: 421-432 (extracellular extension of H2), and 552-559 (cytosolic extension of H6). As for GPER to model the insertions, the following portions: 219-230 (C-terminal portion of E2 and initial portion of H5), 222-225 (in E2), 259-263 and 270-273 (both in I3), and 307-311 (in E3) were deleted in the template crystal structure, followed by addition of external α-helical restraints to the following amino acid stretches: 52-62 (cytosolic half of H1), 226-233 (cytosolic extension of H5), 241-244 (cytosolic extension of H6), 271-278 (extracellular extension of H6), and 286-293 (extracellular extension of H7). For each receptor, one-hundred models were built by randomizing all the Cartesian coordinates of standard residues in the initial model. The best model according to quality checks was subjected to application of rotamer libraries to those side chains in non-allowed conformation.

Prediction of likely architectures of FSHR-GPER heterodimer followed a computational approach developed for quaternary structure predictions of transmembrane α-helical proteins, defined as a FiPD-based approach (Casciari et al., 2006; Fanelli et al., 2013). It consists in rigid-body docking using a version of the ZDOCK program devoid of desolvation as a component of the docking score (v2.1) (Chen et al., 2003). FSHR was used as a fixed protein (target) and GPER as a mobile protein (probe) and vice versa in two distinct docking runs. A rotational sampling interval of 6º was set (i.e., dense sampling) and the best 4000 solutions were retained and ranked according to the ZDOCK score. Such solutions were filtered according to the “membrane topology” filter (by using the FiPD software (Casciari et al., 2006), which discards all those solutions that violate the membrane topology requirements. The membrane topology filter, indeed, discards all the solutions characterized by a deviation

angle from the original z-axis, i.e. tilt angle, and a displacement of the geometrical centre along the z-axis, i.e. z-offset, above defined threshold values, which were 0.4 radians and 6.0 Å, respectively. The filtered solutions from each run were merged with the target protein, leading to an equivalent number of dimers that were clustered using a C_α-RMSD threshold of 3.0 Å for each pair of superimposed dimers. All the amino acid residues in the dimer were included in C_α-RMSD calculations. Cluster analysis was based on a QT-like clustering algorithm (Heyer et al., 1999) implemented both in the FiPD and Wordom software (Casciari et al., 2006; Seeber et al., 2011). Since the filtering cutoffs of the membrane topology parameters are intentionally quite permissive, inspection of the cluster centres (i.e. the solutions with the highest number of neighbours in each cluster) served as a final filter to discard remaining false positives, thereby leading to a dramatic reduction of the reliable solutions. The best scored docking solutions from the most populated and reliable clusters were finally considered. Cluster reliability was based on the MemTop score, accounting for the goodness of the membrane topology. Such index is defined according to the following formula:

$$MemTop = \sqrt{\left\langle tilt_{nor} \right\rangle^2 + \left\langle Z_{offnor} \right\rangle^2}$$

where, the squared terms are, respectively, the normalized tilt angle and the z-offset averaged over all the members of a given cluster. Normalization of each tilt angle and z-offset value was carried out by dividing each value for the respective cutoff value, i.e. 0.4 radians, for the tilt angle, and 6.0 Å, for the z-offset. The optimal value for such index is zero.

Final selection of the likely heterodimer relied on a consensus from the two different docking runs.

CRISPR/Cas9 experiments.

Since AKAP5 is encoded by a single exon (exon 2), two guide RNA probes (gRNAs) were used to excise the entire genetic region (PubMed Gene ID: 9495; last update: 1 June 2020). gRNAs were designed using Benchling platform and then ordered as a synthetic DNA fragment (Gene Strings, Thermo Fisher Scientific) flanked

by two restriction enzyme BbsI recognition sites. Each of the two double-stranded DNA fragment was then cloned into a pSpCas9(BB)-2A-Puro (PX459) V2.0 vector, respectively, which was a gift from Feng Zhang (#62988; Addgene, Watertown, MA, USA), using digestion/ligation protocol (Ran et al., 2013). The vectors were then amplified and purified from ampicillin-resistant bacteria with Zyppy Mini Plasmid Kit (Zymo Research, Irvine, CA, USA).

HEK293 cells transfection was performed using TurboFect reagent (Thermo Fisher Scientific) according to manufacturer protocol. After 48 h, we enriched cell media by 1.2 µg/ml puromycin before to verify the KO by PCR reaction in single clone lysates.

Immunofluorescence and immunohistochemistry.

FSHR and GPER expression was detected by immunofluorescent microscopy in both granulosa and 48-h transfected HEK293 cells using a ZOE Fluorescent Cell Imager (Bio-Rad Laboratories Inc.). Granulosa cells were fixed by 3-min treatment with 4% ice-cold paraformaldehyde/PBS, heated 20 s x 600 W in a microwave and incubated with 20 µg/ml rabbit anti-FSHR (#PA5-28764; ThermoFisher Scientific) and/or 20 µg/ml goat anti-GPER (#LS-B5132; LifeSpan BioSciences, Inc., Seattle, WA, USA) primary antibodies. Secondary antibodies were donkey anti-rabbit FITC and anti-goat TRITC (#ab6798 and #ab6882; Abcam). In transfected HEK293 cells, treatment by the anti-GPER and proper secondary antibody was performed, while FSHR was identified by the venus-tag emission. 300 nM DAPI was used for staining nuclei.

Immunohistochemistry was performed using an R.T.U. Vectastain Universal Elite ABC kit and DBA Substrate Kit (both from Vector Laboratories, Burlingame, CA, USA) according to the manufacturer's instructions. Briefly, paraffin-embedded ovarian tissues of fertile women at the follicular stage, stored in a pathological anatomy laboratory, were sliced into 5 µm sections, deparaffinized and hydrated using decreasing concentration of ethanol. Antigen retrieval was performed by heating sections for 10 min in sodium citrate buffer (pH = 6.0), followed by cooling at room temperature. After treatment for 10 min with 3% hydrogen peroxide in deionized water to quench endogenous peroxidases and for 30 min with normal horse serum (NHS) (Vector Laboratories, Burlingame, CA), sections were incubated overnight at 4°C with primary antibodies diluted in 0.3% NHS in

PBS: 20 µg/ml rabbit anti-FSHR (#PA5-28764; ThermoFisher Scientific, Waltham, MA, USA) or 20 µg/ml rabbit anti-GPER (#LS-A4271; LifeSpan BioSciences Inc., Seattle, WA, USA). Control sections were incubated with 0.3% NHS in PBS in the absence of primary antibody. Slides were incubated in biotinylated horse anti-rabbit (Vector Laboratories, Burlingame, CA) for 30 min at RT followed by 30 min in Elite ABC reagent (Vector Laboratories, Burlingame, CA). Visualization of antibody binding was achieved applying DAB solution (Vector Laboratories, Burlingame, CA) for 5 min. Sections were then counterstained with hematoxylin, dehydrated and mounted using a non-aqueous mounting medium. Images were acquired by Zeiss Axioplan 2 microscope equipped with a Nikon Digital Sight camera.

Proximity ligation assay.

FSHR and GPER interaction was confirmed by proximity ligation assay (PLA) in human primary granulosa cells. Samples were seeded on glass slides and fixed by 4% ice-cold paraformaldehyde/PBS before to be incubated with 20 µg/ml rabbit anti-FSHR (#PA5-28764; ThermoFisher Scientific) and/or 20 µg/ml goat anti-GPER (#LS-B5132; LifeSpan BioSciences, Inc.) primary antibodies. Cells were washed twice with PBS after each protocol step. PLA was applied using the Duolink® In Situ Red Starter Goat/Rabbit kit and following the supplier instructions (#DUO92105-1KT; Sigma-Aldrich). Briefly, samples were incubated 1 h with anti-goat and -rabbit secondary antibodies bound to short DNA strands. These compounds are called “PLUS” and “MINUS” PLA probes and their DNA strands can interact through a subsequent addition of two other circle-forming DNA oligonucleotides whether they are in close proximity (<40 nm). The two oligonucleotides were joined by enzymatic ligation and amplified using a polymerase, forming a rolling circle DNA. Several-hundredfold replications of the DNA circle occur and labeled complementary oligonucleotide probes highlight the product. Therefore, the resulting high concentration light emission may be visible with a fluorescence microscope and indicates the interaction between the two targets. Negative controls were prepared by incubation of samples without the “PLUS”, the “MINUS” probe or the primary antibodies. Slides were then closed using a mounting medium containing DAPI and provided in the PLA kit. Images were acquired using the ZOE Fluorescent Cell Imager (Bio-Rad Laboratories Inc.).

Gene expression and DNA sequencing analysis.

Gene expressions were evaluated using specific primer sequences. *FSHR* (NM_000145.3): fwd 5′-GGAGGTGATAGAGGCAGATG-3′; rev 5′-GGGTTGATGTAGAGCAGGT- 3′; *GPER* (AF027956): fwd 5'-CTGAACCGCTTCTGTCAC-3'; rev 5'-ACTGCTGAACCTCACATC-3'. The *RPS7* housekeeping gene was the loading control (NM_001011.4; fwd: 5'-AATCTTTGTTCCCGTTCCTCA-3'; rev 5'-CGAGTTGGCTTAGGCAGAA-3'). Primers were validated by PCR and DNA Sanger sequencing (Figure S2), performed using known settings (Lazzaretti et al., 2019).

Flow Cytometry.

HEK293 cells were transiently transfected with either plasmid encoding for empty pcDNA3.1 vector (mock) or increasing concentrations of FLAG-tagged FSHR- or untagged GPER-encoding plasmids. To evaluate the relative expression and localization of FSHR and GPER proteins in the cell membrane, cells were also co-transfected with a fixed concentration of FLAG-tagged FSHR- and increasing concentrations of GPER-encoding plasmids. Cells were detached, washed and resuspended in working buffer (PBS without Ca^{2+} and Mg^{2+}; 1% BSA, 2 mM EDTA) 48 hours after transfection. Then, cells were incubated with phycoerythrin (PE)-conjugated anti-FLAG antibody (anti-DYKDDDDK-PE, #130-101-577; 1:100 dilution; Milteny Biotech, Bergisch Gladbach, Germany), 1 h at 4°C, to reveal membrane expression of FSHR. GPER cell membrane expression was revealed by incubating transfected cells 2 h at 4°C with anti-GPER primary antibody (#LS-A4271; LifeSpan BioSciences Inc.) followed by incubation with secondary antibody Alexa Fluor 647-conjugated AffiniPure (1:100 dilution; #AS075 Jackson Laboratory, Bar Harbor, USA), 1 h at 4°C. Cells were washed twice and re-suspended in working buffer before analysis with MACSQuant Analyzer 10 Flow cytometer (Milteny Biotech). Data were analysed and plotted with the FlowJo software (FlowJo, Ashland, OR, USA).

Statistical analysis.

The D'Agostino and Pearson normality test was performed before choosing to use parametric or non-parametric statistics. Two groups of samples were compared

using Mann-Whitney's U-test or t-test, while multiple groups were compared using Kruskal-Wallis or one-/two-way ANOVA as proper, as well as proper post-tests and corrections for multiple comparisons depending on the nature of data. Groups were represented in column graph using box and whiskers plots. Non-linear and linear regressions were used for data interpolation in x-y graphs and two linear regressions were compared using the parallelism test of slopes. Statistics were performed using the GraphPad Prism 6.0 software (GraphPad Software Inc., La Jolla, CA, USA).

Supplementary references

Albanito, L., Sisci, D., Aquila, S., Brunelli, E., Vivacqua, A., Madeo, A., Lappano, R., Pandey, D.P., Picard, D., Mauro, L., et al. (2008). Epidermal Growth Factor Induces G Protein-Coupled Receptor 30 Expression in Estrogen Receptor-Negative Breast Cancer Cells. Endocrinology *149*, 3799–3808.

Bates, B., Zhang, L., Nawoschik, S., Kodangattil, S., Tseng, E., Kopsco, D., Kramer, A., Shan, Q., Taylor, N., Johnson, J., et al. (2006). Characterization of Gpr101 expression and G-protein coupling selectivity. Brain Res. *1087*, 1–14.

Brigante, G., Riccetti, L., Lazzaretti, C., Rofrano, L., Sperduti, S., Potì, F., Diazzi, C., Prodam, F., Guaraldi, G., Lania, A.G., et al. (2019). Abacavir, nevirapine, and ritonavir modulate intracellular calcium levels without affecting GHRH-mediated growth hormone secretion in somatotropic cells in vitro. Mol. Cell. Endocrinol. *482*, 37–44.

Casarini, L., Lispi, M., Longobardi, S., Milosa, F., La Marca, A., Tagliasacchi, D., Pignatti, E., and Simoni, M. (2012). LH and hCG Action on the Same Receptor Results in Quantitatively and Qualitatively Different Intracellular Signalling. PLoS One *7*, e46682.

Casarini, L., Reiter, E., and Simoni, M. (2016). β-arrestins regulate gonadotropin receptor-mediated cell proliferation and apoptosis by controlling different FSHR or LHCGR intracellular signaling in the hGL5 cell line. Mol. Cell. Endocrinol. *437*, 11–21.

Casarini, L., Riccetti, L., De Pascali, F., Gilioli, L., Marino, M., Vecchi, E., Morini, D., Nicoli, A., La Sala, G.B., and Simoni, M. (2017). Estrogen Modulates Specific Life and Death Signals Induced by LH and hCG in Human Primary Granulosa Cells In Vitro. Int. J. Mol. Sci. *18*, 926.

Casarini, L., Riccetti, L., Limoncella, S., Lazzaretti, C., Barbagallo, F., Pacifico, S., Guerrini, R., Tagliavini, S., Trenti, T., Simoni, M., et al. (2019). Probing the Effect of Sildenafil on Progesterone and Testosterone Production by an Intracellular FRET/BRET Combined Approach. Biochemistry *58*, 799–808.

Casciari, D., Seeber, M., and Fanelli, F. (2006). Quaternary structure predictions of transmembrane proteins starting from the monomer: a docking-based approach. BMC

Bioinformatics *7*, 340.

Chen, R., Li, L., and Weng, Z. (2003). ZDOCK: An initial-stage protein-docking algorithm. Proteins Struct. Funct. Genet. *52*, 80–87.

Cheng, S.-B., Dong, J., Pang, Y., LaRocca, J., Hixon, M., Thomas, P., and Filardo, E.J. (2014). Anatomical location and redistribution of G protein-coupled estrogen receptor-1 during the estrus cycle in mouse kidney and specific binding to estrogens but not aldosterone. Mol. Cell. Endocrinol. *382*, 950–959.

Fanelli, F., and De Benedetti, P.G. (2011). Update 1 of: computational modeling approaches to structure-function analysis of G protein-coupled receptors. Chem. Rev. *111*, PR438-535.

Fanelli, F., Seeber, M., Felline, A., Casciari, D., and Raimondi, F. (2013). Quaternary structure predictions and structural communication features of GPCR dimers. Prog. Mol. Biol. Transl. Sci. *117*, 105–142.

Ferraretti, A.P., La Marca, A., Fauser, B.C.J.M., Tarlatzis, B., Nargund, G., Gianaroli, L., and ESHRE working group on Poor Ovarian Response Definition (2011). ESHRE consensus on the definition of “poor response” to ovarian stimulation for in vitro fertilization: the Bologna criteria. Hum. Reprod. *26*, 1616–1624.

Heyer, L.J., Kruglyak, S., and Yooseph, S. (1999). Exploring expression data: identification and analysis of coexpressed genes. Genome Res. *9*, 1106–1115.

Jonas, K.C., Fanelli, F., Huhtaniemi, I.T., and Hanyaloglu, A.C. (2015). Single Molecule Analysis of Functionally Asymmetric G Protein-coupled Receptor (GPCR) Oligomers Reveals Diverse Spatial and Structural Assemblies. J. Biol. Chem. *290*, 3875–3892.

Lazzaretti, C., Riccetti, L., Sperduti, S., Anzivino, C., Brigante, G., De Pascali, F., Potì, F., Rovei, V., Restagno, G., Mari, C., et al. (2019). Inferring biallelism of two FSH receptor mutations associated with spontaneous ovarian hyperstimulation syndrome by evaluating FSH, LH and HCG cross-activity. Reprod. Biomed. Online *38*, 816–824.

Polyzos, N.P., and Sunkara, S.K. (2015). Sub-optimal responders following controlled ovarian stimulation: an overlooked group? Hum. Reprod. *30*, 2005–2008.

Ran, F.A., Hsu, P.D., Wright, J., Agarwala, V., Scott, D.A., and Zhang, F. (2013). Genome engineering using the CRISPR-Cas9 system. Nat. Protoc. *8*, 2281–2308.

Riccetti, L., Yvinec, R., Klett, D., Gallay, N., Combarnous, Y., Reiter, E., Simoni, M., Casarini, L., and Ayoub, M.A. (2017a). Human Luteinizing Hormone and Chorionic Gonadotropin Display Biased Agonism at the LH and LH/CG Receptors. Sci. Rep. *7*, 940.

Riccetti, L., Klett, D., Ayoub, M.A., Boulo, T., Pignatti, E., Tagliavini, S., Varani, M., Trenti, T., Nicoli, A., Capodanno, F., et al. (2017b). Heterogeneous hCG and hMG commercial preparations result in different intracellular signalling but induce a similar long-term progesterone response in vitro. MHR Basic Sci. Reprod. Med. *23*, 685–697.

Riccetti, L., Sperduti, S., Lazzaretti, C., Klett, D., De Pascali, F., Paradiso, E., Limoncella, S., Potì, F., Tagliavini, S., Trenti, T., et al. (2019). Glycosylation Pattern and in vitro Bioactivity of Reference Follitropin alfa and Biosimilars. Front. Endocrinol. (Lausanne). *10*, 503.

Roberts, C.J., Williams, P.M., Davies, J., Dawkes, A.C., Sefton, J., Edwards, J.C., Haymes, A.G., Bestwick, C., Davies, M.C., and Tendler, S.J.B. (1995). Real-Space Differentiation of IgG and IgM Antibodies Deposited on Microtiter Wells by Scanning Force Microscopy. Langmuir *11*, 1822–1826.

Sali, A., and Blundell, T.L. (1993). Comparative protein modelling by satisfaction of spatial restraints. J. Mol. Biol. *234*, 779–815.

Sanz, G., Leray, I., Muscat, A., Acquistapace, A., Cui, T., Rivière, J., Vincent-Naulleau, S., Giandomenico, V., and Mir, L.M. (2017). Gallein, a Gβγ subunit signalling inhibitor, inhibits metastatic spread of tumour cells expressing OR51E2 and exposed to its odorant ligand. BMC Res. Notes *10*, 541.

Seeber, M., Felline, A., Raimondi, F., Muff, S., Friedman, R., Rao, F., Caflisch, A., and Fanelli, F. (2011). Wordom: a user-friendly program for the analysis of molecular structures, trajectories, and free energy surfaces. J. Comput. Chem. *32*, 1183–1194.

Sposini, S., Caltabiano, G., Hanyaloglu, A.C., and Miele, R. (2015). Identification of transmembrane domains that regulate spatial arrangements and activity of prokineticin

receptor 2 dimers. Mol. Cell. Endocrinol. *399*, 362–372.

Wakeling, A.E., Dukes, M., and Bowler, J. (1991). A potent specific pure antiestrogen with clinical potential. Cancer Res. *51*, 3867–3873.

Wan, Q., Okashah, N., Inoue, A., Nehmé, R., Carpenter, B., Tate, C.G., and Lambert, N.A. (2018). Mini G protein probes for active G protein–coupled receptors (GPCRs) in live cells. J. Biol. Chem. *293*, 7466–7473.